Subspace Predictive Control for Vertical Axis Wind Turbines

Haoyue Wen

Master of Science Thesis

TU Delft Delft University of Technology

Delft Center for Systems and Control

Subspace Predictive Control for Vertical Axis Wind Turbines

Master of Science Thesis

For the degree of Master of Science in Systems and Control at Delft University of Technology

Haoyue Wen

April 18, 2022

Faculty of Mechanical, Maritime and Materials Engineering (3mE) · Delft University of Technology

Abstract

Nowadays, with the current environmental crisis, it is critical to make the transition from a fossil fuel driven society to one based on renewable energy. With a constant increase in the installed power capacity, wind energy is playing a crucial role in the global renewable energy mix. To extract energy from wind, both Horizontal Axis Wind Turbine (HAWT)s and Vertical Axis Wind Turbine (VAWT)s are used. Different from the HAWT, the axis of rotation of the VAWT is perpendicular to the ground. This vertical design offers some unique advantages for the VAWT. For example, the generator of the VAWT is located on the ground, hence the maintenance costs are lower compared to the HAWT. Furthermore, the VAWT can be upscaled easier than the HAWT to harvest more energy from a single turbine. These benefits demonstrate the potential of VAWTs for offshore applications. However, the VAWT's blade suffers from periodic aerodynamic loads from the periodically varying Angle of Attack (AOA), and unsteady aerodynamic phenomena, which harm the durability and hence the economic feasibility of the VAWT.

This thesis aims at resolving the blade loads mitigation problem of the VAWT. For wind turbines, pitching the blade is a common way to reduce the loads on the blade. There have been studies done that focus on the power maximization for the VAWT. However, research on the pitch control system for load reduction is lacking. To tackle the blade loads mitigation problem, a data-driven approach called Subspace Predictive Control (SPC) is used to control the individual pitch actuation of a two-bladed 1.5 m H-Darrieus VAWT.

This closed-loop control strategy consists of two parts, an online identification block and an optimal control law based on the identified system. The online identification method applied is called Recursive Predictor-Based Subspace Identification (RPBSID). It can estimate the system parameters online by using the input and output data collected from the VAWT system. Then, two different types of controllers are designed to reduce the blade loads. In the first approach, the constrained Model Predictive Control (MPC) is used. The optimal control input is calculated by solving a finite horizon constrained optimization problem. The individual pitch control action can be automatically adapted based on the online identified model. In the second approach, a Linear-Quadratic Regulator (LQR) is used as a comparison to the

first approach. The LQR solves an infinite horizon unconstrained optimization problem to obtain the optimal state-feedback law. The control gain can be calculated analytically.

Both approaches are first tested on a Simulink model, which is based on the interpolation of lookup tables computed by the Actuator Cylinder (AC) model and blade element theory. Under a stepwise wind condition, the SPC approach shows the potential to reduce the normal load on each blade. It is also found that the MPC is more robust and easier to implement, compared to the LQR. Then, the MPC based SPC is applied to a mid-fidelity simulation tool called Qblade to acquire more realistic results. The controlled pitch trajectory shows good load reduction results under both uniform and turbulent wind conditions. The work presented in this thesis provides a control strategy to reduce the blade loads on VAWTs following a data-driven manner and demonstrates the capability of MPC based SPC in VAWTs' application.

Table of Contents

List of Figures

List of Tables

Preface

Global warming and other environmental problems have become the most critical topic for the world now. Being able to use the MSc system and control knowledge to wind energy application is very exciting. After having an interesting discussion with the author's current supervisor, prof. dr. ir. J.W. van Wingerden, the idea of the thesis subject, "Subspace Predictive Control for Vertical Axis Wind Turbines" is born.

Acknowledgements

I would like to thank my supervisor J.W. van Wingerden for his assistance during the writing of this thesis. Also, my daily supervisor Dr. Yichao Liu and Livia Brandetti have helped me a lot throughout the project. Thanks for the company of my friends from Beemo and Bongo. And special thanks to my friend Emre for the support all the way. Thanks to Song for which we grew together. Finally, I thank my family for their unconditional love.

Delft, University of Technology Haoyue Wen
April 18, 2022

"Do not go gentle into that good night,
Old age should burn and rave at close of day;
Rage, rage against the dying of the light."

— *Dylan Marlais Thomas*

Chapter 1

Introduction

1-1 Research Context

Because of the great demand for energy and the concerning pollution caused by fossil fuels, renewable energy has gained more and more attention over the past decades [10]. As shown in figure 1-1, wind energy is considered the most fast-rising renewable energy in terms of global installation. According to the Global wind report 2021 [1], offshore wind energy installation only contributes to 5% of the total wind energy installation in 2021. This is because the complexity of the technical requirements and the high energy price limit the development of offshore wind energy [11]. However, offshore wind turbine installations are expected to increase in the near future because this technology has several advantages compared to the onshore one [1, 12]:

- higher wind speed, resulting in higher energy production per unit installed.
- less turbulent wind field, allowing the single wind turbine to operate more efficiently.
- availability of large areas, which are suitable for the installation of large wind farms.

Compared to onshore wind turbines, one of the most significant differences for offshore wind turbines is the support structure. In figure 1-2, different types of support structures and the corresponding water depths are illustrated. In Europe, most offshore wind farms are located in the coastal area, with an average water depth of 27.2 m [13]. Hence, monopile, jacket and tripod supporting structures are the most used ones for offshore wind farms. However, a floating structure is needed if the wind turbines are installed in the deep sea with a water depth larger than 50 m, where more wind resources can be observed. Due to the high center of gravity and large rotor swept area of commercial Horizontal Axis Wind Turbine (HAWT)s, the floating foundation may cause a severe tilting problem [14]. An alternative solution to this problem is represented by the VAWT. Different from HAWTs, the axis of rotation of a Vertical Axis Wind Turbine (VAWT) is vertical and perpendicular to the ground. Because of

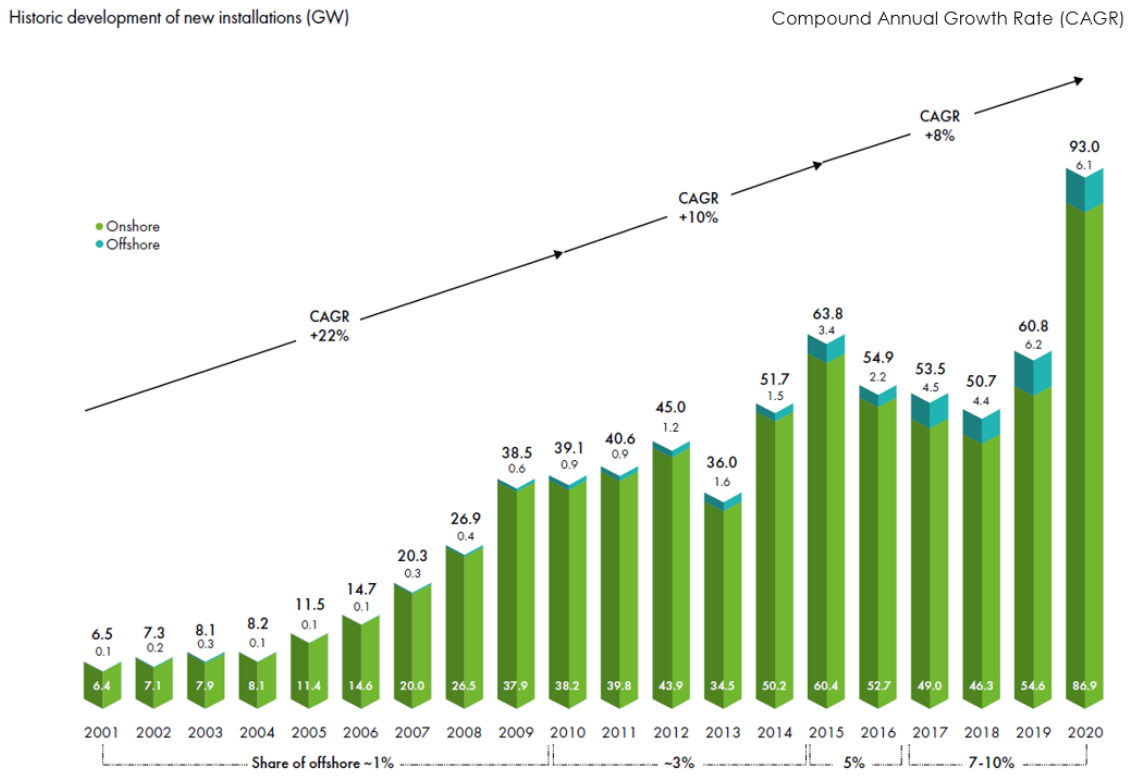

Figure 1-1: Historic development of wind turbine new installations [1]

this vertical design, the heavy electrical components can be located on the ground. This causes the maintenance to be easier and lowers the center of gravity [15]. Further, the VAWT is omnidirectional, hence does not need a yaw system [16]. These advantages make VAWTs more suitable for offshore installation with floating foundations. However, the VAWT experiences periodic aerodynamic loads which cause the fatigue issue [17]. Furthermore, unsteady effects (i.e., blade-wake interaction) occur during the operation of the VAWT, due to the continuous variation of the force field and inflow perceived by the blades. These unsteady aerodynamics also contribute to the fatigue failure of VAWTs [16]. To reduce the aerodynamic loads, blade optimization and flow control have been used [18]. These techniques are generally called passive control. The loads on the turbine blades can also be reduced by pitching the blades, which is called active control [9]. For this approach, a control algorithm needs to be applied to decide the individual pitch angle of the VAWT.

1-2 State of the Art

Through the literature survey, several VAWT projects have been studied [19–21], where different wind turbine configurations have been built and tested. Based on these studies, early fatigue failure is found as a common problem for VAWTs. To gain a better understanding of VAWTs and solve the load problem, researchers mostly focus on analyzing the aerodynamic performance of VAWTs [22–24]. There is also research work on the control strategies of VAWTs, however only achieves the goal of power production maximization [25–27]. The

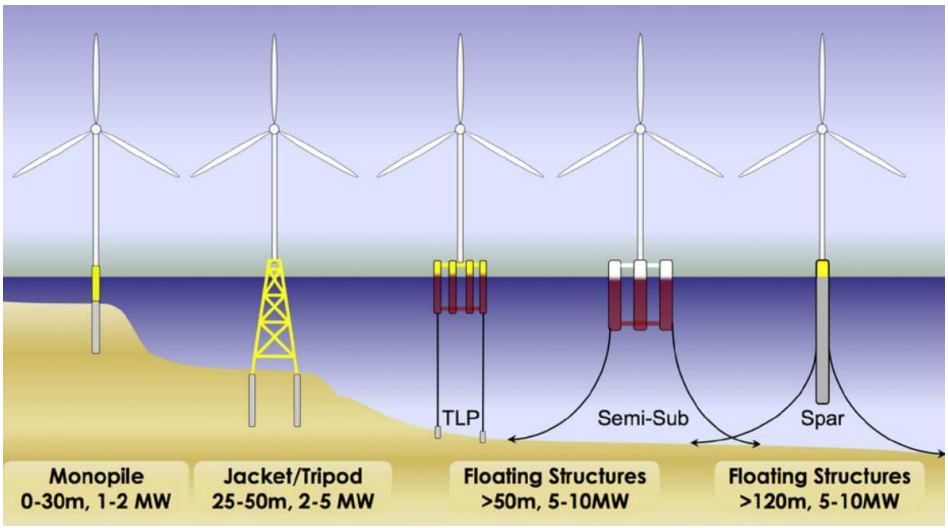

Figure 1-2: Different foundations for offshore wind turbines [2]

lack of load reduction control related research for the VAWT creates a scientific gap that this thesis contributes to filling.

The model-based approach is often used to build the controller for both HAWTs and VAWTs. The system model is built by linearizing the aerodynamic and structure equations at a fixed operating point [28]. However, the linearized model fails to include the nonlinearity of the wind turbine [29]. Further, the wind turbine works at different wind speeds, which makes it a time-varying system. Hence, the linearized model is not capable of fully representing the dynamics of a complex system such as a wind turbine [30]. Lap-Arparat in his study [26] obtains the characteristic curve of the VAWT based on the experimental data. Then, the rotor speed is controlled to reach the optimal TSR according to the characteristic curve. However, the controller is only valid under the given range of wind speed. A gain-scheduled pitch controller is applied based on the Linear Parameter Varying (LPV) system in Bundi's research [25]. The pitch control succeeds to track the designed power curve when the inflow wind speed is above the rated speed. However, since the turbulent and non-linear aerodynamics are difficult to predict, it is impossible to design a single LPV, which works optimally for the wind turbine. Based on the above-mentioned literature [25, 26], the model-based control approach for the VAWT fails to fully represent the nonlinear system, and it is not valid for the entire operating region.

The data-driven approach provides another way to design the controller. Following this approach, the system dynamics are identified through the persistent excitation of the input, i.e., the pitch angle. Then, the controller is designed based on the identified model. Compared to the model-based approach, the data-driven approach does not need a complex linearization and provides reliable system parameters. Besides, the data-driven approach can deal with a time-varying system and adjust the controller accordingly. Through the literature study, the Subspace Predictive Control (SPC) method [31] is found to have the potential of solving the loads mitigation problem of VAWTs. In Navalkar's research [32], the Subspace Predictive

Repetitive Control (SPRC) method shows promising results in rejecting the periodic disturbance of HAWTs. Further, the SPRC is also applied for VAWTs to solve the loads mitigation problem in the master thesis of Vimanyu [33]. However, the SPRC is only valid for periodic disturbance rejection with an accurate value of the period-time. Also, in [33], the controlled pitch trajectories are only validated using a Double Multiple Streamtube Model (DMST) model. The cylindrical swept area of the VAWT is represented by several actuator discs in this method. For this reason, it can not fully represent the VAWT aerodynamics. A more realistic model needs to be applied to further validate the control system.

1-3 Research Questions and Objectives

To reduce the load on blades for wind turbines, the Individual Pitch Control (IPC) is often applied [32]. Using this method, the system dynamics need to be provided to design the control law for individual pitch actuation. However, the dynamics of the VAWT are more complex than the HAWT and highly nonlinear, due to unsteady phenomena such as blade-wake interaction [34]. For this reason, in the current study, the linearisation of the VAWT model is avoided by applying a data-driven approach. Furthermore, an online identification method is applied to capture the time-varying dynamics of the system and improve the effective range of the individual pitch controller. Based on the identified VAWT model, an optimal control law can be synthesised. Following the data-driven approach, the closed-loop control system based on SPC has provided promising results for HAWTs [35]. Showing a great potential to reduce the loads on wind turbines, the SPC method has not been tested and validated for VAWTs in a three-dimensional simulation environment. In this context, the two objectives for this thesis are listed below:

- ***Designing a closed-loop control system that reduces the blade loads on a VAWT under variable operating conditions***. This closed-loop system should be able to identify the VAWT system online under a changing operating condition, such as a changing wind speed. Coupled with the identification block, the individual pitch controller needs to be designed to adjust the pitch actuation according to the online estimated model. For the control strategy, both Model Predictive Control (MPC) and Linear-Quadratic Regulator (LQR) will be applied to reduce the blade normal loads of the VAWT.

- ***Proving the feasibility of the individual pitch control system for VAWT on a mid-fidelity software Qblade***. To simulate the closed-loop control system in a more realistic scenario, Qblade is used [5]. It couples a more accurate aerodynamic model based on Lifting Line Theory (LLT) with a structural dynamics model. Hence, the turbine can be modeled in a three-dimensional environment by performing aeroelastic simulations. A more realistic turbulent wind profile can also be applied. Further, a turbine supervisory controller can be integrated in a Dynamic-Link Library (DLL) format into the Qblade simulations. The results from Qblade can validate the presented control system for reducing the blade loads of the VAWT following the data-driven manner.

1-4 Outline

The research outline is presented blew:

- **Chapter 2** provides an overview of several aerodynamic models of the VAWT: the streamtube model, used for building the Simulink model; the Actuator Cylinder (AC) model, which models the VAWT with a better representation of the swept area; the LLT, which serves as the theoretical foundation for Qblade aerodynamic simulations.
- **Chapter 3** describes the control framework used in this thesis. The details of the algorithm will be provided. The online identification block based on Recursive Predictor-Based Subspace Identification (RPBSID) will be explained first. Then, MPC and LQR will be introduced as two different controllers to close the loop and achieve the load reduction goal. Finally, the working principles of Qblade and how it is connected to the external controller will be shortly explained.
- **Chapter 4** presents the results when the closed-loop control system is applied to the Simulink model. Two control approaches, MPC based SPC and LQR based SPC are compared based on the results. Then, the SPC framework is validated on Qblade.
- **Chapter 5** summarizes the results provided in the previous chapter, which answers the research questions for this thesis. The controlled pitch trajectories achieve a significant load reduction performance for the VAWT. Further, recommendations for possible future work are presented.

Chapter 2

Aerodynamics of Vertical Axis Wind Turbines

In this chapter, the aerodynamics of the Vertical Axis Wind Turbine (VAWT) will be described. First, the working principles of the VAWT will be analyzed by providing a comparison with the well-known Horizontal Axis Wind Turbine (HAWT). Then, three aerodynamic models including streamtube model, blade element method and Actuator Cylinder (AC) model will be reviewed. Further, a Simulink model is formulated to calculate the normal force on the blade based on the blade element method. It uses the induction factor calculated from the thrust coefficient, which is interpolated from the lookup tables given by the author's daily supervisor. The lookup tables are calculated by the AC model. Then, the Lifting Line Theory (LLT) is introduced, which serves as the theoretical foundation for the aerodynamic simulation performed in Qblade [5]. Following this, the overall workflow of Qblade will also be briefly introduced.

2-1 Working Principles of Vertical Axis Wind Turbines

To describe the VAWT, the azimuth angle needs to be introduced first. As shown in figure 2-1, the upwind part of the rotor is defined from 0 to 180 degrees, while the downwind part is defined from 180 to 360 degrees. The blade moves from upwind to downwind part periodically, resulting in a periodic Angle of Attack (AOA) as a function of the azimuth angle. The AOA α of the VAWT blades can be expressed as [36]

$$\alpha = \tan^{-1}\left(\frac{(1-a)\sin\theta}{(1-a)\cos\theta+\lambda}\right)-\beta, \tag{2-1}$$

where λ is the Tip-Speed Ratio (TSR), θ is the azimuth angle, and β is the pitch angle which is defined as the angle between the airfoil chord line and the tangent of the rotational path.

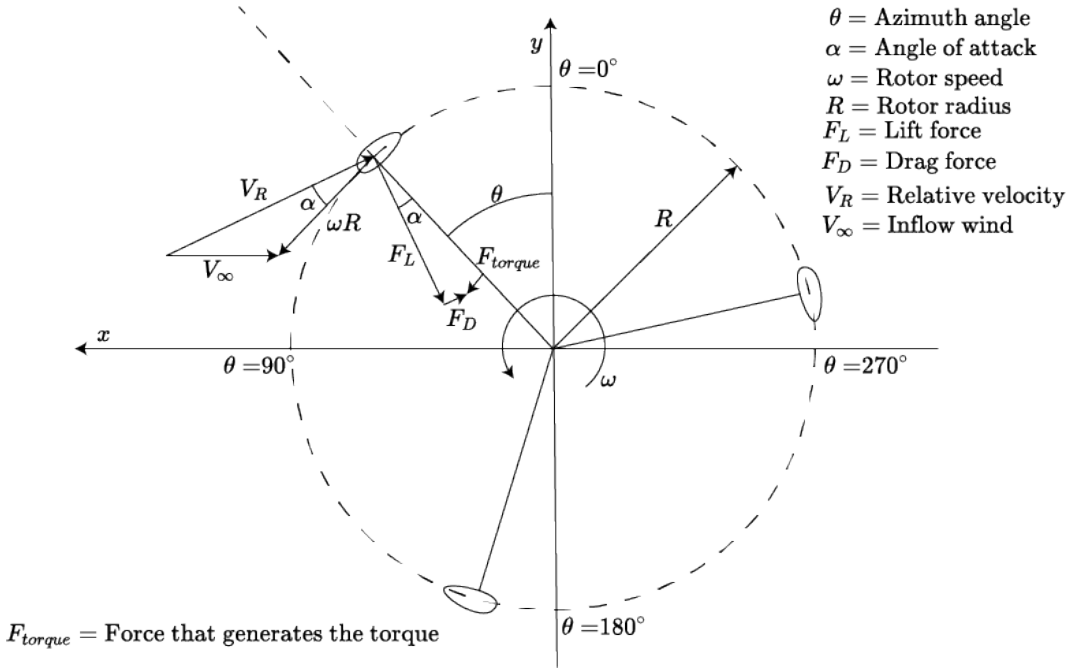

Figure 2-1: Diagram of the blade loading on a lift-type vertical axis wind turbine rotor adapted from the PhD thesis of Pearson [3]

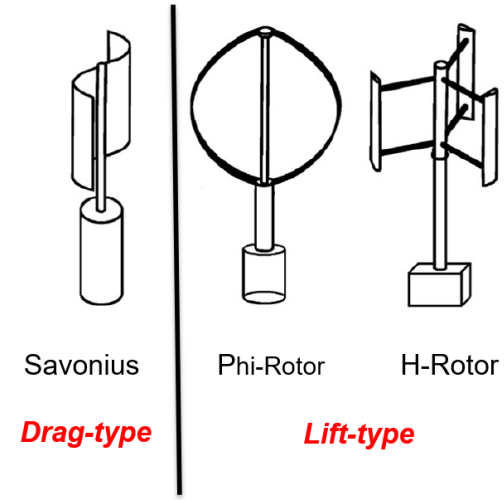

Figure 2-2: Different types of the vertical axis wind turbine [4]

Furthermore, there are mainly two different types of VAWT, as illustrated in figure 2-2. The drag-type converts the torque from a component of the drag force that is in the same direction as the blade movement, while the lift-type acquires the torque from the component of the lift force that is in the direction of the rotation as shown in figure 2-1. Although the drag-type VAWT has several advantages, such as a good starting torque [37], the lower power coefficient with respect to the lift-type VAWT limits its development [38]. Hence, most research work focuses on the lift-type VAWTs which mainly consist of Phi-rotor VAWT and H-rotor VAWT. Through the literature study, it is found that the H-rotor VAWTs have some advantages compared to Phi-rotor VAWTs as listed:

- The operation range of Phi-rotor VAWTs is reduced to avoid the vibration problem of the guy wire.
- Phi-rotor VAWTs suffer from the gravity-induced bending stress because there is no strut to support the blade.
- The long curved blade requires more investment to endure the severe loads condition in the offshore environment.

For these reasons, the wind turbine under study is the H-rotor VAWT in this thesis.

2-2 Aerodynamic Models

2-2-1 Streamtube Model

In this section, one of the simplest streamtube models is introduced: the so-called actuator disk model. Figure 2-3 shows how this model works [36].

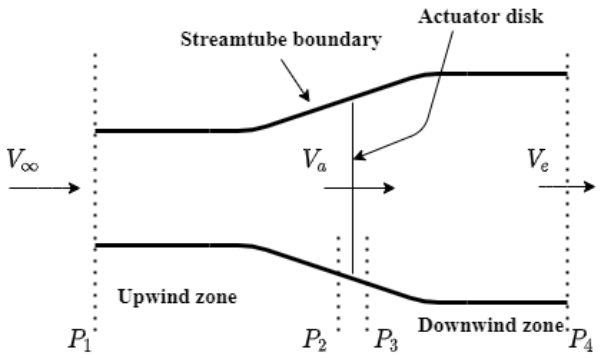

Figure 2-3: Actuator disk model. The inflow wind V_∞ is induced at the actuator disk. The induced velocity V_a at the rotor plane decreases to V_e at the downstream. P_1, P_2, P_3 and P_4 denote the pressure at different positions.

The actuator disk extracts the energy when the flow travels through it. The momentum and energy loss of the flow is caused by the thrust force. To calculate it, the conservation equations of mass, momentum and energy are applied. Furthermore, there are some assumptions for the actuator disk model as listed below [39]:

- The fluid condition is ideal and static.
- The analysis using this model is one-dimensional.
- The disc is infinitesimally thin.
- The thrust force is uniformly distributed through the entire disc.

First, analyzing the upstream part of the disk and applying the Bernoulli equation, the pressure and velocity relation can be described as

$$P_1 + 1/2\rho V_\infty^2 = P_2 + 1/2\rho V_a^2, \tag{2-2}$$

where P_1 is the pressure of the far upwind part, P_2 is the pressure of the upwind part of the actuator disk, V_a is the induced velocity, V_∞ is the inflow wind speed, and ρ is the air density. In the downstream part of the disk, the Bernoulli equation is expressed as

$$P_3 + 1/2\rho V_a^2 = P_4 + 1/2\rho V_e^2, \tag{2-3}$$

where P_3 is the pressure of the downwind part of the actuator disk, P_4 is the pressure of the far downwind part and V_e is the downstream velocity. In this model, far upstream and downstream pressure is assumed to be equal ($P_1 = P_4$), and the velocity is continuous. The thrust force T that is uniformly distributed on the disk, which is expressed as

$$T = A(P_2 - P_3), \tag{2-4}$$

where A is the area of the actuator disk. The difference of the pressure $P_2 - P_3$ can be solved with equation (2-2) and equation (2-3). Then, substituting the result of $P_2 - P_3$ to equation (2-4), the thrust force can be expressed as

$$T = 1/2\rho A(V_\infty^2 - V_e^2). \tag{2-5}$$

Using the momentum theory, the thrust force can also be expressed as

$$T = \rho A V_a(V_\infty - V_e) = m(V_\infty - V_e), \tag{2-6}$$

where $m = \rho A V_a$ is the mass flow rate. Equating equation (2-5) and (2-6), the velocity at the actuator disk plane is expressed as

$$V_a = (V_\infty + V_e)/2. \tag{2-7}$$

The induction factor a is defined as

$$a = (V_\infty - V_a)/V_\infty. \tag{2-8}$$

Using the induction factor, the induced wind velocity and the velocity at downstream can be expressed as

$$V_a = V_\infty(1-a), \tag{2-9}$$

and

$$V_e = V_\infty(1-2a). \tag{2-10}$$

Substituting (2-9) and (2-10) in equation (2-5), the thrust can be expressed as

$$T = 1/2\rho A V_\infty^2 \left[4a(1-a)\right]. \tag{2-11}$$

The non-dimensional thrust coefficient C_T can be expressed as

$$C_T = \frac{T}{1/2\rho A V_\infty^2} = 4a(1-a). \tag{2-12}$$

2-2-2 Blade Element Method

The blade element method is used to calculate the aerodynamic force applied to the blade, and it discretizes the blade into several two-dimensional airfoil sections as shown in figure 2-4 [5].

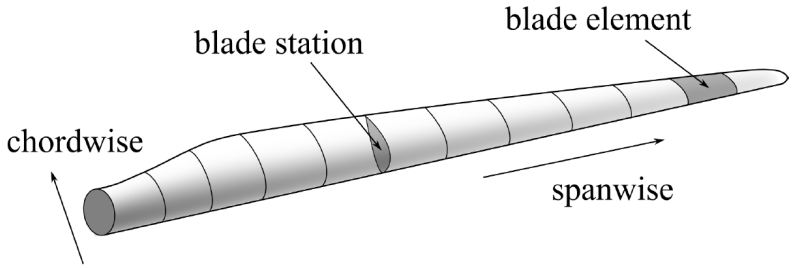

Figure 2-4: The discretized blade using the blade element method [5]

At each section, the aerodynamic force is analyzed as shown in figure 2-1. Using the velocity field at the rotor plane and the azimuth angle of the blade, the normal force acting on the blade section can be calculated. First, the relative velocity V_R of the blade can be expressed as

$$V_R = \sqrt{(V_a \sin\theta)^2 + (V_a \cos\theta + \omega R)^2}, \tag{2-13}$$

where θ is the azimuth angle, R is the rotor radius, and ω is the rotational speed. The AOA α can be expressed as

$$\begin{aligned}\tan(\alpha+\beta) &= \frac{V_a \sin\theta}{V_a \cos\theta + \alpha R} \\ \tan(\alpha+\beta) &= \frac{\frac{V_a}{V_\infty}\sin\theta}{\frac{V_a}{V_\infty}\cos\theta + \frac{\omega R}{V_\infty}} \\ \alpha &= \tan^{-1}\left(\frac{(1-a)\sin\theta}{(1-a)\cos\theta + \lambda}\right) - \beta.\end{aligned} \tag{2-14}$$

The convention for the pitch angle β is given in figure 2-5.

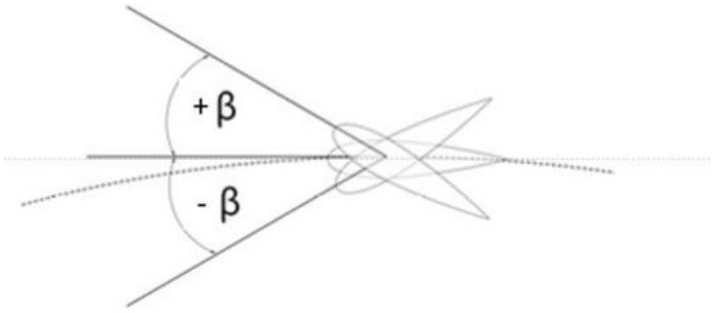

Figure 2-5: Pitch convention applied to the blade, where the pitch angle is positive when the airfoil chord line turns outside the rotor plane and negative when the chord line turns inside it

After computing the AOA, the normal coefficient C_n and tangential coefficient C_t can be calculated as

$$\begin{aligned}C_\mathrm{n} &= C_\mathrm{L}\cos\alpha + C_\mathrm{D}\sin\alpha, \\ C_\mathrm{t} &= C_\mathrm{L}\sin\alpha - C_\mathrm{D}\cos\alpha,\end{aligned} \tag{2-15}$$

where C_L and C_D are the lift and drag coefficients obtained by interpolating the lookup table of the given airfoil. The normal force F_n is expressed as

$$F_\mathrm{n} = 1/2\rho V_R^2 hc(C_\mathrm{n}\cos\beta - C_\mathrm{t}\sin\beta), \tag{2-16}$$

where h is the blade height and c is the blade chord length.

2-2-3 Actuator Cylinder Model

As discussed in section 2-2-1, the actuator disk model considers the wind turbine as a thin disk. However, for the VAWT, the swept surface is cylindrical, which can be perceived as omnidirectional. To better represent the surface geometry of the VAWT, the Actuator Cylinder

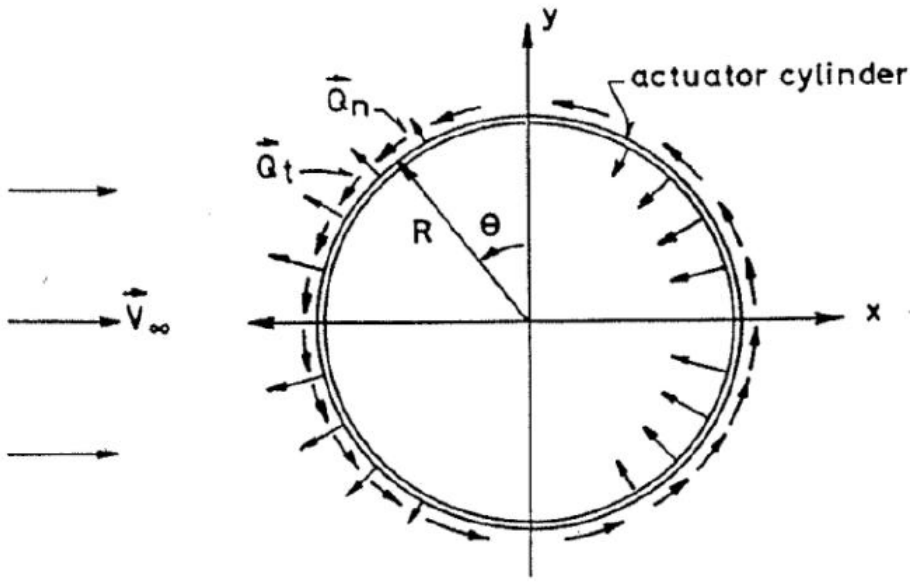

Figure 2-6: Actuator Cylinder model representation, with Q_n being the normal loading, Q_t the tangential loading, R the radius of the turbine, θ the azimuth angle and V_∞ the inflow wind speed [6]

(AC) model is introduced by Madsen in his PhD thesis [40].

The reaction of the blade forces in the AC model are applied on the flow field as volume forces perpendicular and tangential to the rotor plane as shown in figure 2-6 [6]. The normal loading Q_n and tangential loading Q_t are defined as

$$\begin{aligned} Q_n(\theta) &= N\frac{F_n(\theta)\cos(\beta) - F_t(\theta)\sin(\beta)}{2\pi R} \\ Q_t(\theta) &= -N\frac{F_t(\theta)\cos(\beta) + F_n(\theta)\sin(\beta)}{2\pi R}, \end{aligned} \tag{2-17}$$

where N is the number of blades, F_n is the blade force per unit length perpendicular to the cord, and F_t is the blade force per unit length parallel to the chord. Further, the volume forces f_n and f_t are defined as

$$\begin{aligned} Q_n(\theta) &= \lim_{\epsilon\to 0}\int_{R-\epsilon}^{R+\epsilon} f_n(\theta)ds \\ Q_t(\theta) &= \lim_{\epsilon\to 0}\int_{R-\epsilon}^{R+\epsilon} f_t(\theta)ds, \end{aligned} \tag{2-18}$$

where ϵ is a small distance in the radial direction, since the volume forces are non-zero only at the actuator cylinder [41]. Following the blade element method introduced in section 2-2-2, the forces can be calculated from the velocity field. The resulted thrust coefficient C_T is given as

$$C_T = \frac{\int_0^{2\pi}(Q_n(\theta)\sin(\theta) + Q_t(\theta)\cos(\theta))d\theta}{\rho V_\infty^2}. \tag{2-19}$$

To calculate the velocity field using AC model, the velocity is decomposed into two components v_x and v_y which are in the stream-wise and lateral directions, expressed as

$$\begin{aligned} v_x &= 1 + w_x \\ v_y &= w_y, \end{aligned} \tag{2-20}$$

where w_x and w_y are the perturbation velocity in the stream-wise and lateral directions. The Euler equation is expressed as

$$\begin{aligned} \frac{\partial w_x}{\partial x} + w_x\frac{\partial w_x}{\partial x} + w_y\frac{\partial w_x}{\partial y} &= -\frac{\partial p}{\partial x} + f_x \\ \frac{\partial w_y}{\partial x} + w_x\frac{\partial w_y}{\partial x} + w_y\frac{\partial w_y}{\partial y} &= -\frac{\partial p}{\partial y} + f_y, \end{aligned} \tag{2-21}$$

where p is the pressure field, f_x is the volume force in the stream-wise direction, and f_y is the volume force in the lateral direction. The equation of continuity is expressed as

$$\frac{\partial w_x}{\partial x} + \frac{\partial w_y}{\partial y} = 0. \tag{2-22}$$

To derive a Poisson type equation, the equation 2-21 is rewritten as

$$\begin{aligned} \frac{\partial w_x}{\partial x} &= -\frac{\partial p}{\partial x} + f_x + g_x \\ \frac{\partial w_y}{\partial x} &= -\frac{\partial p}{\partial y} + f_y + g_y, \end{aligned} \tag{2-23}$$

where g_x and g_y are the second order volume forces. It can be expressed as

$$\begin{aligned} g_x &= -\left(w_x\frac{\partial w_x}{\partial x} + w_y\frac{\partial w_x}{\partial y}\right) \\ g_y &= -\left({}_x\frac{\partial w_y}{\partial x} + w_y\frac{\partial w_y}{\partial y}\right). \end{aligned} \tag{2-24}$$

Inserting the momentum equation 2-23 into the continuity equation 2-22 and differentiating the resulted equation in x-direction and y-direction, the equation 2-23 can be rewritten as

$$\frac{\partial^2 p}{\partial x^2} + \frac{\partial^2 p}{\partial y^2} = \frac{\partial f_x}{\partial x} + \frac{\partial f_y}{\partial y} + \frac{\partial g_x}{\partial x} + \frac{\partial g_y}{\partial y}. \tag{2-25}$$

The boundary condition is defined as the pressure goes to zero when x and y go to infinity. Using the boundary condition, the pressure equation is then expressed as

$$\begin{aligned} p(f) &= \frac{1}{2\pi}\int\int \frac{f_x(x-\xi) + f_y(y-\eta)}{(x-\xi)^2 + (y-\eta)^2}d\xi d\eta \\ p(g) &= \frac{1}{2\pi}\int\int \frac{g_x(x-\xi) + g_y(y-\eta)}{(x-\xi)^2 + (y-\eta)^2}d\xi d\eta, \end{aligned} \tag{2-26}$$

where ξ and η represent the local coordinates in x and y direction. The total integration of equation (2-26) is divided into several local rectangular elements. After acquiring the pressure field, the velocity can be found by integrating equation (2-23). The result can be presented as a linear part $w(f)$ and a nonlinear part $w(g)$ as

$$\begin{aligned} w_x &= w_x(f) + w_x(g) \\ w_y &= w_y(f) + w_y(g). \end{aligned} \tag{2-27}$$

The resulted linear solutions for the velocity field are expressed as

$$\begin{aligned} w_x = &- \frac{1}{2\pi}\int_0^{2\pi} Q_n(\theta)\frac{-x(x+\sin(\theta))\sin(\theta) + (y-\cos(\theta))\cos(\theta)}{(x+\sin(\theta))^2 + (y-\cos(\theta))^2}d\theta \\ &- Q_n(\arccos(y))^* + Q_n(-\arccos(y))^{**} \\ w_y = &- \frac{1}{2\pi}\int_0^{2\pi} Q_n(\theta)\frac{-x(x+\sin(\theta))\cos(\theta) - (y-\cos(\theta))\sin(\theta)}{(x+\sin(\theta))^2 + (y-\cos(\theta))^2}d\theta, \end{aligned} \tag{2-28}$$

where the * term is the only term calculated within the actuator cylinder, and the * and ** terms are both calculated in the wake behind the actuator cylinder. The interested reader is referred to Madsen's PhD thesis [40] for the full derivation.

2-3 Simulink Model Formulation

To test the control algorithm, a Simulink model is built to simulate the blade loads of the VAWT. This Simulink model is a 2D model. It is based on the induction factor calculated from the thrust coefficient, which is interpolated from the lookup tables. The lookup tables of pitch angle, tip-speed ratio, power coefficient, and torque coefficient used in the formulation are provided by the author's daily supervisor and calculated with the AC model. Following the assumption of the streamtube model, the induced velocity is considered uniform at the rotor plane. Then, the aerodynamic force can be calculated using the blade element method with the induced velocity.

The overall workflow for the Simulink VAWT model is shown in figure 2-7. For a given pitch angle, wind speed and rotor speed, the thrust coefficient can be calculated based on a linear interpolation of the lookup table. After the thrust coefficient is obtained, the induction factor can be calculated based on equation (2-12). Using the induction factor, the velocity information at the rotor plane can be obtained. The lift coefficient and drag coefficient can be obtained by interpolating the database for the given type of airfoil based on the calculated AOA. Then, the normal force on the blade section can be calculated following the blade element method through equation (2-13) to equation (2-16).

For the two-bladed H-rotor VAWT studied in this thesis, a Multi Input Multi Output (MIMO) system can be presented as given in figure 2-8 by modeling two single blades without dynamics coupling. The blade 2 is shifted with respect to blade 1 by 180 degrees. This Simulink model works under these assumptions:

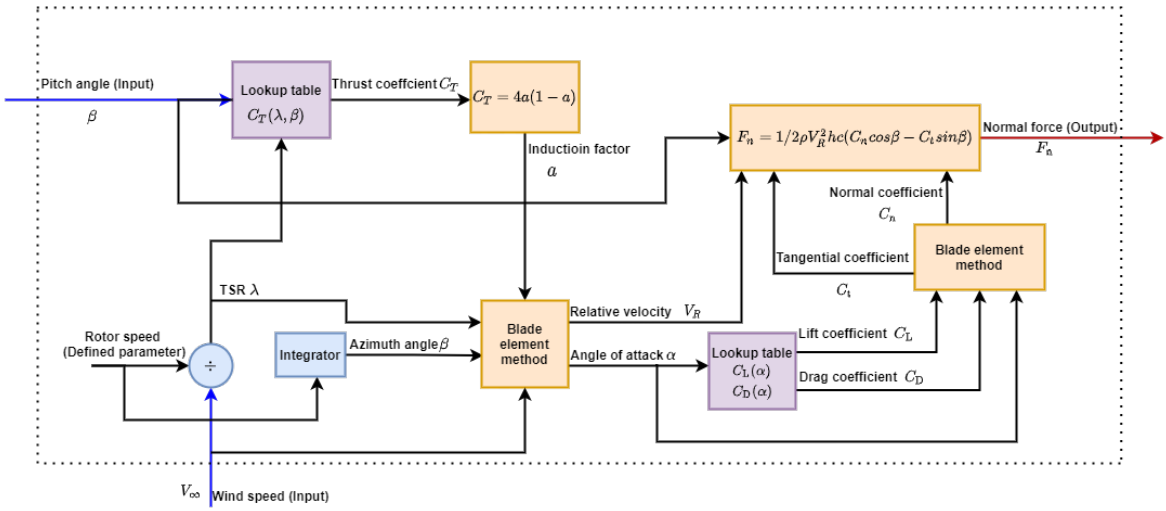

Figure 2-7: Workflow of Simulink VAWT model, where wind speed V_∞ and pitch angle β are the inputs, and normal force F_n is the output. The thrust coefficient C_T is first interpolated from the lookup table. Then, the induction factor a is calculated from the thrust coefficient based on the actuator disk model. Further, the normal force F_n is calculated using the velocity information and following the blade element method

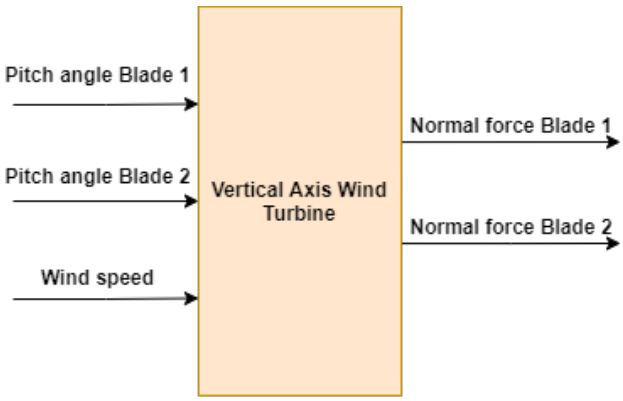

Figure 2-8: Inputs and outputs of the Simulink model

- The rotor speed is kept constant.
- The TSR is kept within the range of the lookup table (1 - 4.5).
- The pitch actuation is assumed to be ideal (i.e., the pitch actuator works at the same frequency as the discrete-time model with a sample time of 0.01 s and there is no delay for the pitch actuator).

2-4 Lifting Line Theory

In section 2-2, several aerodynamic models are introduced which are based on the conservation of mass, momentum and energy. This kind of method works under several assumptions: a static and ideal flow condition; the blades are always inside the rotor plane; the rotor plane is always oriented to the incoming flow [5]. However, these assumptions are violated in a realistic condition, i.e., the blade has deflections that make it not work in the rotor plane. To give a more accurate aerodynamic prediction, the Lifting Line Theory (LLT) is introduced. A brief overview of LLT is provided in this section. For further details, the interested reader is referred to [5, 7]. The aerodynamic model based on LLT is implemented in Qblade together with a structural model [5]. The full turbine can be simulated in a three-dimensional environment. In this way, a more realistic scenario can be simulated.

The LLT assumes that the generated lift on the blade surface acts at the quarter of the chord. Hence, the rotor is represented by a lifting line located at the quarter of the chord. Then, the blade is discretized into several blade panels. Each blade panel is represented by a ring vortex composed of four vortex line elements as shown in figure 2-9 [5].

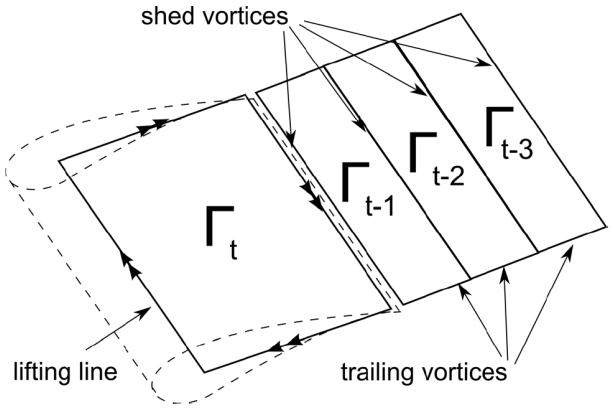

Figure 2-9: Geometry of a blade panel, position of the lifting line, and shed and trailing vortex line elements [5]

The induced velocity is calculated from the vorticity field. Further, the lift and drag coefficient can be obtained from the induced AOA. Finally, the load on the blade can be calculated based on the LLT. The following iteration algorithm is used to compute the vorticity field:

- Assuming a distribution of the vortex strength Γ.

- Calculating the onset velocity $\vec{u}_{cp}$ for each blade panel on its control point as a combination of the inflow wind $\vec{u}_{wind}$, the blade motion $\vec{u}_{motion}$, and the induced vorticity $\vec{u}_{\Gamma}$.

$$\vec{u}_{cp} = \vec{u}_{wind} + \vec{u}_{motion} + \vec{u}_{\Gamma}. \tag{2-29}$$

The induced vorticity can be calculated as

$$\vec{u}_{\Gamma} = \frac{\Gamma}{4\pi} \frac{(r_1 + r_2)(\vec{r_1} \times \vec{r_2})}{r_1 r_2 (r_1 r_2 + \vec{r_1} \cdot \vec{r_2} + (\delta l_0)^2}, \tag{2-30}$$

where l_0 is the length of the vortex line and δ is a cut-off factor to imply the velocity induction when vortex line length increases. $\vec{r_1}$ and $\vec{r_2}$ are the position vectors as shown in figure 2-10.

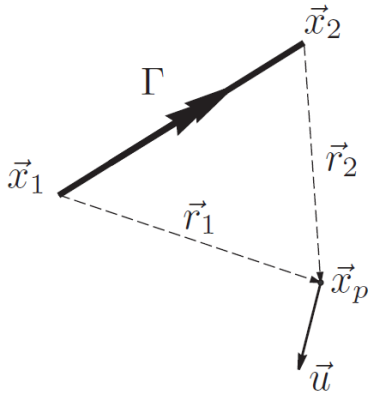

Figure 2-10: Vortex line geometry of the control point, where $\vec{r_1}$ and $\vec{r_2}$ are the position vectors from the vortex line that starts at position $\vec{x_1}$ and end at position $\vec{x_2}$ to the evaluation point $\vec{x_p}$ [7]

- Calculating the local angle of attack α_{cp} for the control point of each blade panel as

$$\alpha_{cp} = \arctan\left(\frac{\vec{u}_{cp} \cdot \vec{a}_3}{\vec{u}_{cp} \cdot \vec{a}_1}\right), \tag{2-31}$$

where $\vec{a}_1$ and $\vec{a}_3$ are the unit vectors in the chordwise and normal directions.

- Using the airfoil data table to determine the lift coefficient C_{L} for each blade panel according to the given angle of attack.

- Computing a new guess of vortex strength Γ_{cl} based on the lift coefficient as

$$\Gamma_{cl} = C_{\mathrm{L}} \frac{0.5((\vec{u}_{cp} \cdot \vec{a}_1)^2 + (\vec{u}_{cp} \cdot \vec{a}_3)^2) dA_s}{\sqrt{((\vec{u}_{cp} \times d\vec{l}) \cdot \vec{a}_1)^2 + ((\vec{u}_{cp} \times d\vec{l}) \cdot \vec{a}_3)^2}}, \tag{2-32}$$

where A_s is the strip area.

- Calculating the difference of vortex strength $\triangle\Gamma$ between the initial guess Γ and the new guess Γ_{cl} as

$$\triangle\Gamma = \Gamma_{cl} - \Gamma. \tag{2-33}$$

- Adding this difference of vortex strength to the initial guess Γ with a under-relaxation factor θ as

$$\Gamma = \Gamma + \theta\triangle\Gamma. \tag{2-34}$$

- The convergence criterion is defined as a function of maximum occurring vortex strength $\mid \Gamma \mid_{max}$ and the difference value of vortex strength $\triangle\Gamma$, expressed as

$$\frac{\mid \triangle\Gamma \mid}{\mid \Gamma \mid_{max} +1} > \Gamma_{crit}. \tag{2-35}$$

  If the convergence criterion is not met, return to the first step.

In Qblade, after the LLT method convergence, the algorithm moves to the next time step. The rotor rotates, and all vortex elements are convected with the local inflow wind V_{wind} and local induced velocity V_Γ. There are two methods to iterate the wake convection step. To calculate the convected vortex node x_{t+1}, the first-order method is given as [5]

$$x_{t+1} = x_t + (V_{\text{wind}} + V_\Gamma(x_t))\triangle t. \tag{2-36}$$

The second-order method using a predictor corrector is given as

$$x_{t+1,cor} = x_t + (2V_{\text{wind}} + V_\Gamma(x_t) + V_\Gamma(x_{t+1}))\frac{\triangle t}{2}. \tag{2-37}$$

As the iteration evolves, a new vortex element is formed between the trailing edge of each blade panel, and the last vortex element is convected from the trailing edge. This iteration step is calculated using the Kutta condition.

$$\begin{aligned} \Gamma_{trail} &= \frac{\partial\Gamma_{bound}}{\partial x}\triangle x \\ \Gamma_{shed} &= \frac{\partial\Gamma_{bound}}{\partial t}\triangle t \end{aligned} \tag{2-38}$$

where Γ_{trail} is the trailing vortex, Γ_{shed} is the shed vortex, and Γ_{bound} is the bound circulation. After the new vortex circulation is computed and assigned, the algorithm goes back to the first step of the LLT method. The overall flow chart of the LLT algorithm applied in Qblade is shown in figure 2-11.

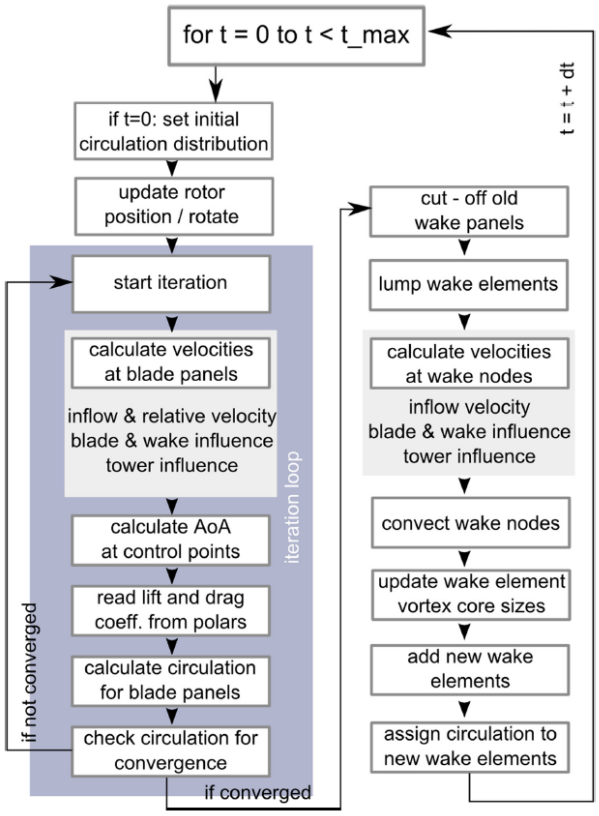

Figure 2-11: Flowchart of Qblade implemented LLT algorithm for one time-step [5]

2-5 Qblade Working Principles

In the previous section, the LLT is introduced, which is implemented in the aerodynamic model of Qblade [5]. Further, the aerodynamic model is coupled with the structural dynamics model to perform the aeroelastic simulation as shown in figure 2-12.

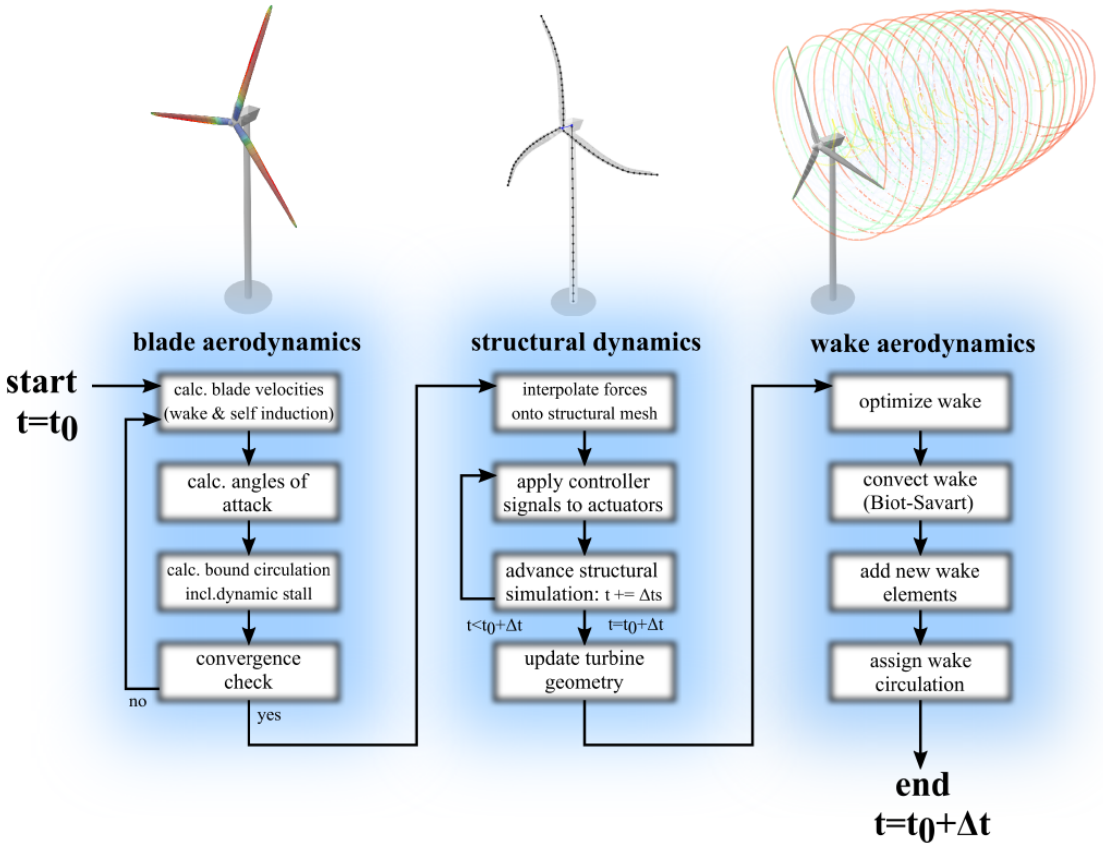

Figure 2-12: Flowchart for one time step of the aeroelastic model in QBlade [5]

The aerodynamic model first calculates the forces and moments on blade panels based on the LLT introduced in section 2-4. Then, the forces and moments are interpolated to the structural mesh. The structural dynamics model in Qblade uses a co-rotational multi-body formulation with Bernoulli beam elements [5]. Further, the control actuation is applied. When the structural simulation finishes advancing, the turbine geometry updates. Then, in the last step, the wake aerodynamics is updated.

Chapter 3

Subspace Predictive Control Framework

In this chapter, a data-driven approach is introduced to reduce the normal load of the Vertical Axis Wind Turbine (VAWT). The general control strategy for wind turbines is introduced first. Then, the traditional subspace identification is illustrated [42]. Further, the Recursive Least Square (RLS) approach is introduced to solve traditional subspace identification online. This method is called Recursive Predictor-Based Subspace Identification (RPBSID) [43], which can identify the VAWT system under a time-varying operating condition. Finally, the Model Predictive Control (MPC) and Linear-Quadratic Regulator (LQR) are designed to close the control loop and solve the loads mitigation problem.

3-1 Wind Turbine Control

The concepts introduced in this section are applicable to both HAWTs and VAWTs. The baseline controllers for wind turbines are used to control the generator torque and the pitch angle in a way that the turbine follows the designed power curve. Figure 3-1 is a schematic representation of the wind turbine power curve. As indicated in figure 3-1, the entire operating region of the wind turbine can be separated into three parts [44]. In the region-1, the wind turbine does not generate power and stays at a standstill or idle state because the wind speed is lower than the cut-in speed. In the region-2, the wind speed is above the cut-in speed, and the generator is switched on but does not operate at its full capacity. Hence, this region is also called the partial load region. When the wind speed reaches the rated speed, the wind turbine operates in the region-3, where the generator is at full load. The region-3 is also called the full load region. When the wind speed exceeds the cut-out speed, the rotor is brought to a standstill.

To track the designed power curve of wind turbines, the baseline control is applied. The full control loop for the wind turbine is shown in 3-2. The torque controller and pitch controller work in different operating regions to ensure that the rotor speed is kept at the desired value.

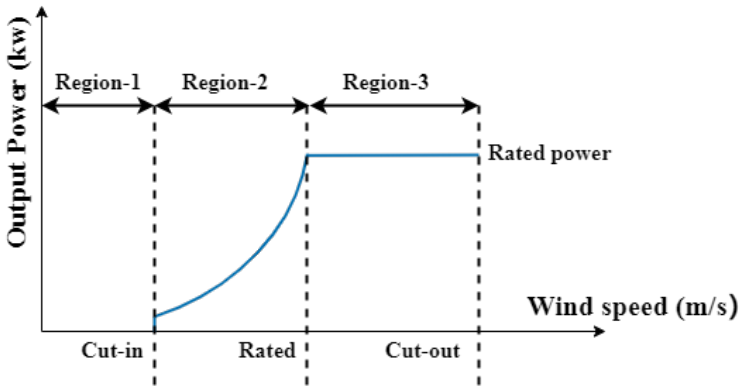

Figure 3-1: Different operating regions of the wind turbine

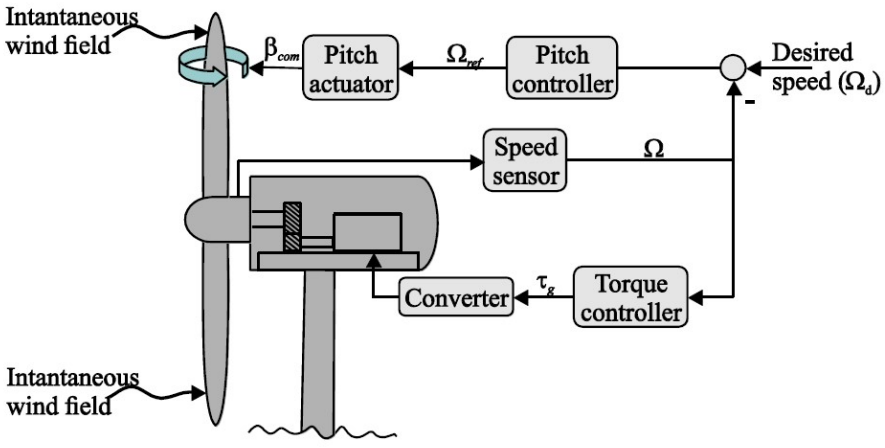

Figure 3-2: Control loop for the wind turbine. The desired rotor speed Ω_d is achieved by controlling the generator torque τ_g in the partial load region and controlling the collective pitch angle β_{com} in the full load region. The measured rotor speed Ω is used as the feedback signal [8]

In the partial load region, the objective of the controller is to maximize power extraction. This is achieved by varying the generator torque to control the generator speed. In the full load region, the pitch controller is activated to keep the power at the rated value. The collective pitch controller is commonly used to solve this task by pitching each blade at the same rate and angle. Notice that, besides the conventional collective pitch control, the Individual Pitch Control (IPC) control is used to reduce the fatigue load of turbines where each blade can pitch independently [8].

3-2 Subspace Identification

3-2-1 Problem Formulation

Before solving the load mitigation problem for the VAWT, the dynamics of the VAWT system need to be identified. The system is considered observable and assumed as a minimal state-space model in the innovation form as [43]

$$\begin{aligned} x_{k+1} &= Ax_k + Bu_k + Ke_k \\ y_k &= Cx_k + Du_k + e_k, \end{aligned} \tag{3-1}$$

where $x(k) \in \mathbb{R}^n$ is the state vector with n dimensions, $u(k) \in \mathbb{R}^r$ is the input vector representing the individual pitch angle with r dimensions, $y(k) \in \mathbb{R}^l$ is the output vector corresponding to the normal load on each blade with l dimensions, and $e(k) \in \mathbb{R}^l$ is the process noise of the system that is assumed to be white noise. Using the system output definition, the original system (3-1) can be rewritten in a predictor form as

$$\begin{aligned} x_{k+1} &= \bar{A}x_k + \bar{B}u_k + Ky_k \\ y_k &= Cx_k + Du_k + e_k, \end{aligned} \tag{3-2}$$

where $\bar{A} = A - KC$, and $\bar{B} = B - KD$. The goal of the subspace identification method is to find all the system matrices A, B, C, D, and K using the input sequence u_k and the output sequence y_k of the system. For the control design, the separated system matrices A, B, C, D, and K are not always needed depending on which controller is used. This will be further explained in section 3-2. The main reason is that the system output can be predicted using the past Inuput/Output (I/O) information and the system Markov matrix.

3-2-2 Notations Definition

To assure the consistency and clarity of this section, some notations need to be defined. First, determining an input sequence and output sequence during a past window $p \in \mathbb{N}^+$ as

$$Z_k = \begin{bmatrix} z_k \\ z_{k+1} \\ \vdots \\ z_{k+p-1} \end{bmatrix}, \tag{3-3}$$

where $z_k = \begin{bmatrix} u_k^T & y_k^T \end{bmatrix}^T$ is a dimension $m = r + l$ vector that consists of the system input and output information. Following the same manner, stacked vectors Z_{k-p}, Y_k, and E_k can be obtained. Some short matrix notations also need to be defined as $\tilde{B} = \begin{bmatrix} \bar{B} & K \end{bmatrix}$, and $\tilde{D} = \begin{bmatrix} D & O \end{bmatrix}$ where O is a l-by-l zero matrix. To build the data equation that carries the relation between system input and output, some block matrices need to be defined as [43]

$$\begin{aligned} \mathcal{O} &= \begin{bmatrix} C \\ C\bar{A} \\ C\bar{A}^2 \\ \vdots \\ C\bar{A}^{p-1} \end{bmatrix}, \mathcal{T} = \begin{bmatrix} \tilde{D} & 0 & 0 & \cdots & 0 \\ C\tilde{B} & \tilde{D} & 0 & \cdots & 0 \\ C\bar{A}\tilde{B} & C\tilde{B} & \tilde{D} & \cdots & 0 \\ \vdots & \vdots & \ddots & \ddots & \vdots \\ C\bar{A}^{p-2}\tilde{B} & C\bar{A}^{p-3}\tilde{B} & \cdots & C\tilde{B} & \tilde{D} \end{bmatrix}, \\ \mathcal{K} &= \begin{bmatrix} \bar{A}^{p-1}\tilde{B} & \bar{A}^{p-2}\tilde{B} & \cdots & \bar{A}\tilde{B} & \tilde{B} \end{bmatrix}, \end{aligned} \tag{3-4}$$

where $\mathcal{O} \in \mathbb{R}^{pl \times n}$ is the extended observability matrix, $\mathcal{T} \in \mathbb{R}^{pl \times pm}$ is a lower block triangular Toeplitz matrix, and $\mathcal{K} \in \mathbb{R}^{pl \times pm}$ is the extended controllability matrix.

3-2-3 System Identification Algorithm

Following the model defined in (3-1) and using the matrices defined in section 3-2-2, the input-output behaviour of the system can be presented as

$$Y_k = \mathcal{O}x_k + \mathcal{T}Z_k + E_k. \tag{3-5}$$

The state vector x_k can be further expressed as

$$x_k = \bar{A}^p x_{k-p} + \mathcal{K}Z_{k-p}. \tag{3-6}$$

Now, an approximation of the state vector x_k is introduced. The main assumption is that for a uniformly exponentially stable system in (3-2), the exponential matrix $\bar{A}^p \approx 0$ when the past window p is large enough [43, 45]. Hence, the state vector x_k can be estimated as

$$x_k \approx \mathcal{K}Z_{k-p}. \tag{3-7}$$

Introducing this state approximation to equation (3-5), the output sequence can be expressed as

$$Y_k \approx \mathcal{O}\mathcal{K}Z_{k-p} + \mathcal{T}Z_k + E_k. \tag{3-8}$$

The product of the state and the extended observability matrix $\mathcal{O}x_k$ can be constructed as

$$\bar{q}_k \triangleq \mathcal{O}\mathcal{K}Z_{k-p} \approx \mathcal{O}x_k. \tag{3-9}$$

Following the assumption made in 3-7, it holds that

$$\lim_{p\to\infty} \bar{q}_k \triangleq \mathcal{O}\mathcal{K}Z_{k-p} = \mathcal{O}x_k. \tag{3-10}$$

To retrieve the state vector x_k, the matrix product $\mathcal{O}\mathcal{K}$ need to be found. Noticing that the matrix product $\mathcal{O}\mathcal{K}$ can be simplified using the assumption that $\bar{A}^k \approx 0$ for all $k \geq p$. The matrix product $\mathcal{O}\mathcal{K}$ is approximated as

$$\begin{aligned}\mathcal{O}\mathcal{K} &= \begin{bmatrix} C\bar{A}^{p-1}\tilde{B} & C\bar{A}^{p-2}\tilde{B} & \cdots & C\tilde{B} \\ C\bar{A}^{p}\tilde{B} & C\bar{A}^{p-1}\tilde{B} & \cdots & C\bar{A}\tilde{B} \\ \vdots & \ddots & \ddots & \vdots \\ C\bar{A}^{2p-1}\tilde{B} & \cdots & C\bar{A}^{p}\tilde{B} & C\bar{A}^{p-1}\tilde{B} \end{bmatrix} \\ &\approx \begin{bmatrix} C\bar{A}^{p-1}\tilde{B} & C\bar{A}^{p-2}\tilde{B} & \cdots & C\tilde{B} \\ 0 & C\bar{A}^{p-1}\tilde{B} & \cdots & C\bar{A}\tilde{B} \\ \vdots & \ddots & \ddots & \vdots \\ 0 & \cdots & 0 & C\bar{A}^{p-1}\tilde{B} \end{bmatrix}.\end{aligned} \tag{3-11}$$

By investigating the approximation made in equation 3-11, it is found that $\mathcal{O}\mathcal{K}$ can be reconstructed by matrix product $C\mathcal{K}$ and zero matrix O as

$$\mathcal{O}\mathcal{K} = \begin{bmatrix} C\mathcal{K} \\ \begin{bmatrix} O^{(r+l)\times(r+l)}, C\mathcal{K}(:, 1:(r+l)(p-1)) \end{bmatrix} \\ \begin{bmatrix} O^{(r+l)\times 2(r+l)}, C\mathcal{K}(:, 1:(r+l)(p-2)) \end{bmatrix} \\ \vdots \\ \begin{bmatrix} O^{(r+l)\times(p-1)(r+l)}, C\mathcal{K}(:, 1:(r+l)) \end{bmatrix} \end{bmatrix}, \tag{3-12}$$

where $C\mathcal{K}(n_r : m_r, n_c : m_c)$ is a Matlab notation used for simplicity. It represents a selected sub-matrix using the original matrix element from row n_r to m_r and column n_c to m_c. Now, the Markov matrix $C\mathcal{K}$ need to be described in a linear problem that can be solved. After analyzing the output behaviour of the system, the least square problem is built as [43]

$$[C\mathcal{K}\ D] = arg\min_{[C\mathcal{K}\ D]} \left\| \bar{Y} - \begin{bmatrix} C\mathcal{K} & D \end{bmatrix} \Psi \right\|_F^2, \tag{3-13}$$

where $\bar{Y}$ and Ψ are stacked vectors constructed as

$$\begin{aligned} \bar{Y} &= \begin{bmatrix} y_{p+1} & y_{p+2} & \cdots & y_N \end{bmatrix} \\ \bar{Z} &= \begin{bmatrix} Z_1 & Z_2 & \cdots & Z_{N-p+1} \end{bmatrix} \\ \Psi &= \begin{bmatrix} \bar{Z}^T & \bar{U}^T \end{bmatrix}^T. \end{aligned} \tag{3-14}$$

Due to the approximation made in equation (3-7), the solution of linear problem (3-13) is biased. However, the bias will be eliminated when the past window p is big enough ($p \to \infty$) [45, 46]. Using the system Markov matrix $[C\mathcal{K}\ D]$, the output of the system can be predicted based on the past I/O data. This output predictor will be used to design the MPC. For LQR, the system matrices A, B, C and D are used, this requires further calculations to get the separated system matrices. Hence, the following part is continued to construct the estimated state vector and build another linear problem to solve the separated system matrices.

After obtaining the value of matrix product $C\mathcal{K}$ by solving the least square problem (3-13), matrix product $\mathcal{O}\mathcal{K}$ can be reconstructed following equation (3-12). Then, the product of the extended observability matrix and state sequence $\mathcal{O}\bar{X}$ of the system can be retrieved using equation (3-7). To acquire the estimated state sequence $\hat{X}$, a singular value decomposition is used as [43]

$$\mathcal{O}\mathcal{K}\bar{Z} \approx \begin{bmatrix} U & U_\perp \end{bmatrix} \begin{bmatrix} \Sigma_n & 0 \\ 0 & \Sigma \end{bmatrix} \begin{bmatrix} V \\ V_\perp \end{bmatrix}, \tag{3-15}$$

where Σ_n is the diagonal matrix that contains the n largest singular values, this value also denotes the dimension of the estimated system state. It can be determined by a gap between the large singular value and the small singular value. Using this diagonal matrix σ_n, the estimated state sequence can be expressed as

$$\hat{X} = \Sigma_n^{\frac{1}{2}} V. \tag{3-16}$$

Furthermore, the system matrices A, B, C, and D can be solved based on the system model (3-1). The least square problem is expressed as

$$\Theta = arg\ \min_{\Theta} \left\| \begin{bmatrix} \bar{X}(:, p+2:N) \\ \bar{Y} \end{bmatrix} - \Theta \begin{bmatrix} \bar{X}(:, p+1:N-1) \\ \bar{U} \end{bmatrix} \right\|_F^2, \tag{3-17}$$

where Θ represents a block matrix containing A, B, C, and D, that is, $\Theta = \begin{bmatrix} A & B \\ C & D \end{bmatrix}$.

3-3 Recursive Predictor-Based Subspace Identification

In section 3-2, two least square problems (3-13) and (3-17) are formulated to solve the system identification problem. To solve this problem online, the Recursive Least Square (RLS) approach is used [47]. The system Markov matrix $[C\mathcal{K}\ D]$ and system matrices A, B, C, D can be solved recursively to adapt to the time-varying system dynamics. For a smaller computational load, the least square problems presented in (3-13) and (3-17) are rewritten in an array form as

$$[C\mathcal{K}\ D] = arg \min_{[C\mathcal{K}\ D]} \left\| y_k - \begin{bmatrix} C\mathcal{K} & D \end{bmatrix} \begin{bmatrix} Z_{k-p} \\ u_k \end{bmatrix} \right\|_F^2, \tag{3-18}$$

and

$$\begin{bmatrix} A & B \\ C & D \end{bmatrix} = arg \min_{\begin{bmatrix} A & B \\ C & D \end{bmatrix}} \left\| \begin{bmatrix} x_k \\ y_{k-1} \end{bmatrix} - \begin{bmatrix} A & B \\ C & D \end{bmatrix} \begin{bmatrix} x_{k-1} \\ u_{k-1} \end{bmatrix} \right\|_F^2. \tag{3-19}$$

After solving (3-18), the estimated state vector need to be constructed to solve (3-19) based on the subspace identification framework. To reduce the computational costs, a different approach is used to estimate the state vector. The propagator method [48], developed by Mercère et al., uses a permutation matrix $S \in \mathbb{R}^{lp \times lp}$ to decompose the extended observability matrix as

$$\begin{bmatrix} \bar{q}_{k,1} \\ \bar{q}_{k,2} \end{bmatrix} \triangleq S\mathcal{O}\mathcal{K}Z_{k-p} = \begin{bmatrix} \mathcal{O}_1 \\ \mathcal{O}_2 \end{bmatrix} \mathcal{K}Z_{k-p} = \begin{bmatrix} I_n \\ P_r \end{bmatrix} \mathcal{O}_1\mathcal{K}Z_{k-p}, \tag{3-20}$$

where $\mathcal{O}_1$ contains the first n independent rows, $\mathcal{O}_2$ includes the rest of the independent rows, and P_r is a unique operator called the propagator. Introducing this decomposition to approximation (3-7), the estimated state vector yield to

$$\hat{x} = \bar{q}_{k,1} \approx \mathcal{O}_1 x_k. \tag{3-21}$$

In [48], a detailed explanation of how to find the permutation matrix S is presented. The permutation matrix S used in the thesis is given as

$$S = \begin{bmatrix} I^{n \times n} & O^{n \times (pl-n)} \end{bmatrix}, \tag{3-22}$$

where I is an identify matrix and O is a zero matrix.

The overall RPBSID algorithm is presented in algorithm 1. The algorithm first solves (3-18) recursively with the forgetting factor λ_f, which denotes the weight on the past and recent data. The value of it is usually taken between 0.98 and 1, where a smaller value results in a faster update rate but less stable performance [49]. After solving the system Markov matrix $[C\mathcal{K}\ D]$, the estimated state vector can be computed using the method present in (3-20) and (3-21). In the last step, linear problem (3-19) is recursively solved to obtain the system matrices A, B, C, D. Then, the algorithm advances, the data sequence updates, and the recursive identification starts again for the next time step. To express these least square problems in a more compact way, it is denoted that $\Theta_1 = \begin{bmatrix} C\mathcal{K} & D \end{bmatrix}$, $\Theta_2 = \begin{bmatrix} A & B \\ C & D \end{bmatrix}$, $\psi = \begin{bmatrix} Z_{k-p} \\ u_k \end{bmatrix}$, $X_f = \begin{bmatrix} x_{k-1} \\ u_{k-1} \end{bmatrix}$, and $X_f^+ = \begin{bmatrix} x_k \\ y_{k-1} \end{bmatrix}$.

3-4 Model Predictive Control Based Subspace Predictive Control

To capture the time-varying dynamics of the VAWT system, an online system identification method called RPBSID is introduced in section 3-3. Using this method, the system Markov

Algorithm 1 Recursive Predictor-Based Subspace Identification Algorithm

$\lambda_f \leftarrow 1$ ▷ Default value for forgetting factor
$P_1, P_2 \leftarrow 0$ ▷ Default value for initial covariance matrix
$x \leftarrow 0$ ▷ Initial value for estimated state vector
$\Theta_1 \leftarrow 0$ ▷ Initial value for estimated system matrices
for $k \geq p+1$ **do**

$$\psi_k = \begin{bmatrix} Z_{k-p} \\ u_k \end{bmatrix}$$

Finding the system Markov matrix Θ_1:

$$P_{1,k} = \frac{1}{\lambda_f}(P_{1,k-1} - \frac{P_{1,k-1}\psi_k\psi_k^T P_{1,k-1}}{\lambda_f + \psi_k^T P_{1,k-1}\psi_k})$$
$$P_{1,k} = \frac{1}{2}(P_{1,k} + P_{1,k}^T)$$
$$e = y_k - \Theta_{1,k-1}\psi_k$$
$$\Theta_{1,k} = \Theta_{1,k-1} + e\psi_k P_{1,k}$$

Estimating state vector:

$$\mathcal{OK}_k = \begin{bmatrix} C\mathcal{K}_k(:, 1:(r+l)p) \\ \left[O^{(r+l)\times(r+l)}, C\mathcal{K}_k(:, 1:(r+l)(p-1))\right] \\ \left[O^{(r+l)\times 2(r+l)}, C\mathcal{K}_k(:, 1:(r+l)(p-2))\right] \\ \vdots \\ \left[O^{(r+l)\times(p-1)(r+l)}, C\mathcal{K}_k(:, 1:(r+l))\right] \end{bmatrix}$$

$$\bar{q}_k = S\mathcal{OK}_k Z_{k-p}$$
$$x_k = \bar{q}_k(1:n, :)$$

Finding the system matrices Θ_2:

$$P_{2,k} = \frac{1}{\lambda_f}(P_{2,k-1} - \frac{P_{2,k-1}X_{f,k}X_{f,k}^T P_{2,k-1}}{\lambda_f + X_{f,k}^T P_{2,k-1}X_{f,k}})$$
$$P_{2,k} = \frac{1}{2}(P_{2,k} + P_{2,k}^T)$$
$$e = X_{f,k}^+ - \Theta_{2,k-1}X_{f,k}$$
$$\Theta_{2,k} = \Theta_{2,k-1} + eX_{f,k}P_{2,k}$$

end for

matrix can be updated online with the forgetting factor. Based on the identified system model, the MPC based Subspace Predictive Control (SPC) method is presented in this section to close the control loop and achieve the loads reduction goal for the VAWT.

Under the RPBSID scheme discussed in the previous section, the one-step future output of the system can be predicted based on the input-output behaviour (3-18) as

$$\hat{y}_k \approx \begin{bmatrix} C\mathcal{K} & D \end{bmatrix} \begin{bmatrix} Z_{k-p} \\ u_k \end{bmatrix}. \tag{3-23}$$

For a multiple prediction horizon f, a more complicated formulation of future output sequence Y_f and future input sequence U_f can be found in algorithm 2.

Algorithm 2 Formulation of an Output Predictor of f Prediction Horizon

$U_f = \begin{bmatrix} u_k \\ \vdots \\ u_{k+c} \\ \vdots \\ u_{k+c} \end{bmatrix}$ ▷ Future input $U \in \mathbb{R}^{fr}$ sequence where $c \leq f$ is the control horizon

$Y_f = \begin{bmatrix} y_k \\ \vdots \\ y_{k+f-1} \end{bmatrix}$ ▷ Future output sequence

$Z \leftarrow Z_{k-p}$

for $1 \leq i \leq f$ **do**

$Y_f(l(i-1)+1 : li, :) = \begin{bmatrix} C\mathcal{K} & D \end{bmatrix} \begin{bmatrix} Z \\ U_f(r(i-1)+1 : ri, :) \end{bmatrix}$

$Z = \begin{bmatrix} Z(mi+1 : end, :) \\ U_f(r(i-1)+1 : ri, :) \\ Y_f(l(i-1)+1 : li, :) \end{bmatrix}$ ▷ The constraint of the system dynamics denote as C_{sys}

end for

To acquire the output sequence of f prediction horizon, the one-step future output y_k is constructed first. Then, the I/O data sequence Z is updated using the one-step future input and output. Further, the second-step future output y_{k+1} can be constructed and the for loop continues. This procedure ends when the designed prediction horizon is reached.

After obtaining the future output sequence, a linear quadratic cost function has to be defined to compute the optimized future control input sequence. For the VAWT system, the control input needs to be constrained since the individual pitch angle can not exceed the design limitation. There is no constraint for the system output, which is the normal load on each blade. It is only penalized by the weighting matrix Q_m. The cost function is presented as

$$\begin{aligned} &\min_{U_f} \quad J = Y_f^T Q_m Y_f + U_f^T R_m U_f \\ &\text{subject to } U_f \in \mathcal{U} \text{ and } C_{sys} \end{aligned} \tag{3-24}$$

where R_m and C_{sys} are the weighting matrix for the control input and the constraint defined in algorithm 2. Because Y_f is the future output sequence which is a linear function of the future input sequence U_f, and weighting matrices Q_m and R_m are positive definite, the cost function J is convex for the design variable U_f. For a constrained control input u_k, it satisfies $lb \leq u_k \leq ub$, where lb and ub are the lower and upper bounds of the control input. This constraint can be written in a compact way as

$$Wu_k \leq a, \tag{3-25}$$

where $W = \begin{bmatrix} I \\ -I \end{bmatrix} \in \mathbb{R}^{2r \times r}$, $a = \begin{bmatrix} ub \\ lb \end{bmatrix} \in \mathbb{R}^{2r \times 1}$. The feasible region $\mathcal{U}$ of the control input sequence U_f can be expressed as

$$\bar{W}U_f \leq \bar{a}, \tag{3-26}$$

where $\bar{W} = I_f \otimes W \in \mathbb{R}^{2rf \times rf}$ and $\bar{a} = \begin{bmatrix} a \\ \vdots \\ a \end{bmatrix} \in \mathbb{R}^{2rf \times 1}$.

After the optimal control input sequence U_f is successfully computed as

$$U_f = \arg\min_{U_f} J \text{ subject to } U_f \in \mathcal{U} \text{ and } C_{sys}, \tag{3-27}$$

the value of the first block $U_f(1:r,:)$ is taken as the control input signal to the individual pitch actuator. The prediction horizon f and control horizon c can be tuned under the regulation $c \leq f \leq p$ where p denotes the past window size. For a large prediction horizon f, the system dynamics are predicted during a long period. This can cause the accumulation of system identification errors. The predicted output sequence is also discarded after the current time step, and the computational load will increase if the prediction horizon f is large. The control horizon c indicates the design variable dimensions for the optimization problem. The quadratic problem solver tends to give a more optimal solution if the control horizon c is larger because there is less constraint on the design variables. On the other side, the actual control input u_k only takes the first entry of the whole future control input sequence U_f, and only the first one or two steps significantly affect the future outputs. Hence, the control horizon c is also recommended to take a small value. The overall block diagram of the closed-loop system using MPC based SPC is shown in figure 3-3.

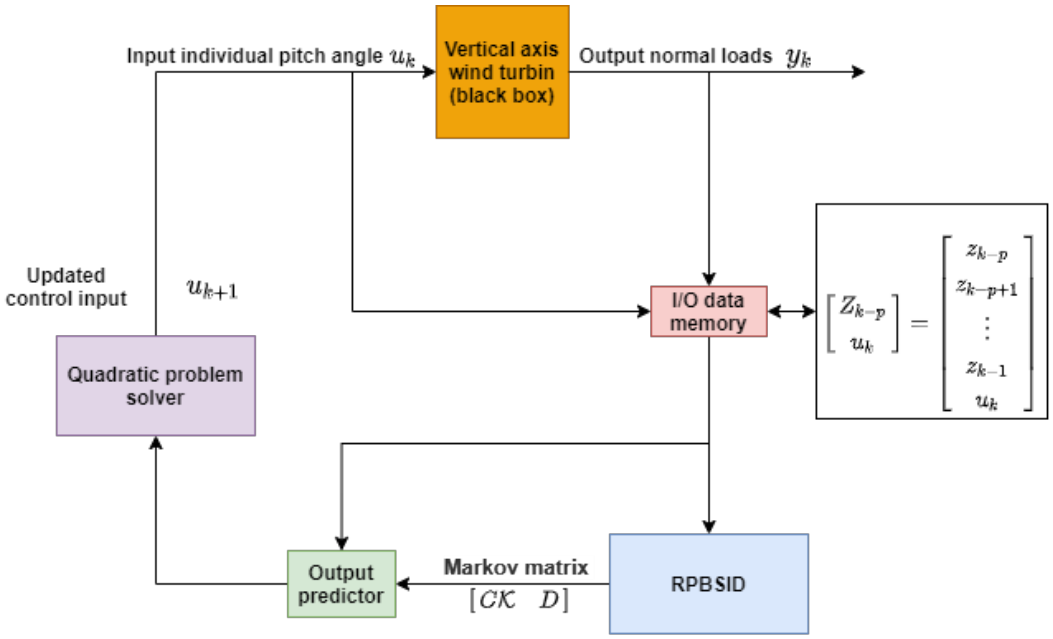

Figure 3-3: Block diagram of the closed-loop system using MPC based SPC

3-5 Linear-Quadratic Regulator Based Subspace Predictive Control

In section 3-3, the RPBSID method is presented to update the identified system matrices A, B, C, and D in every time step. With the system matrices obtained, the VAWT system can be expressed as a discrete-time state-space model given by

$$\begin{aligned} x_{k+1} &= Ax_k + Bu_k \\ y_k &= Cx_k + Du_k. \end{aligned} \tag{3-28}$$

For such a discrete-time system, the LQR is commonly used to drive the state to the origin or reference state by solving a linear-quadratic problem. In this report, the LQR based SPC is used to compare the control performance with the MPC based SPC. The LQR seeks the optimal state feedback gain to minimize the cost function, which expressed as

$$J = \sum_{k=0}^{\infty} x^T Q_l x + u^T R_l u, \tag{3-29}$$

where Q_l and R_l are the weighting matrices for the system states and the control inputs. This cost function formulation is also considered as an infinite-horizon unconstrained optimization problem. No external quadratic problem solver is needed to solve this linear-quadratic problem because there is an analytic solution to this problem. It is found that the optimal control sequence u_k can be expressed by a control gain K_l as

$$u_k = -K_l x_k. \tag{3-30}$$

The control gain K_l can be computed by a positive definite matrix P_l as

$$K_l = (R_l + B^T P_l B)^{-1} B^T P_l A, \tag{3-31}$$

where P_l is the unique positive definite solution of the Discrete-time Algebraic Riccati Equation (DARE) [50]

$$P_l = A^T P_l A - A^T P_l B (R_l + B^T P_l B)^{-1} B^T P_l A + Q_l. \tag{3-32}$$

To recursively solving the DARE at iteration k, the P_l is given as [51]

$$P_{l,k+1} = Q_l + A_k^T (P_{l,k} - P_{l,k} B_k^T (R + B_k^T P_{l,k} B_k)^{-1} B_k^T P_{l,k}) A_k. \tag{3-33}$$

Further, the optimal state feedback gain $K_{l,k}$ is calculated based on equation (3-31) as

$$K_{l,k} = (R + B_k^T P_{l,k} B_k)^{-1} B_k^T P_{l,k} A_k. \tag{3-34}$$

In order to add the possibility to manipulate the convergence characteristics of the algorithm, the a and b is introduced as [51]

$$K_{l,k} = a K_{l,k} + b K_{l,k-1}, \tag{3-35}$$

where $a + b = 1$, and both a and b are positive to assign a weight on the new and old control gain respectively.

The LQR based SPC does not guarantee the feasibility of the control input u_k because it is not constrained as in the MPC based SPC formulation where $u_k \in \mathcal{U}$. The control input can only be penalized by increasing the value of the weighting matrix R_l. The initial value of the weighting matrices is commonly set to an equal value as $Q_l = I$ and $R_l = I$. Then, it is tuned by the power of 10 to increase the penalty on system states or control inputs. Also, the individual entry of weighting matrices can be adjusted to penalize a specific state or control input. Although the system matrices A, B, C, and D are online identified and updated, the weighting matrices Q_l and R_l are tuned as a constant value through simulations which does not automatically update when system dynamics change. This can result in an unfeasible control input since LQR solves an unconstrained optimization problem, hence considered as a disadvantage of the LQR controller. The block diagram of the closed-loop system using the LQR based SPC is shown in figure 3-4.

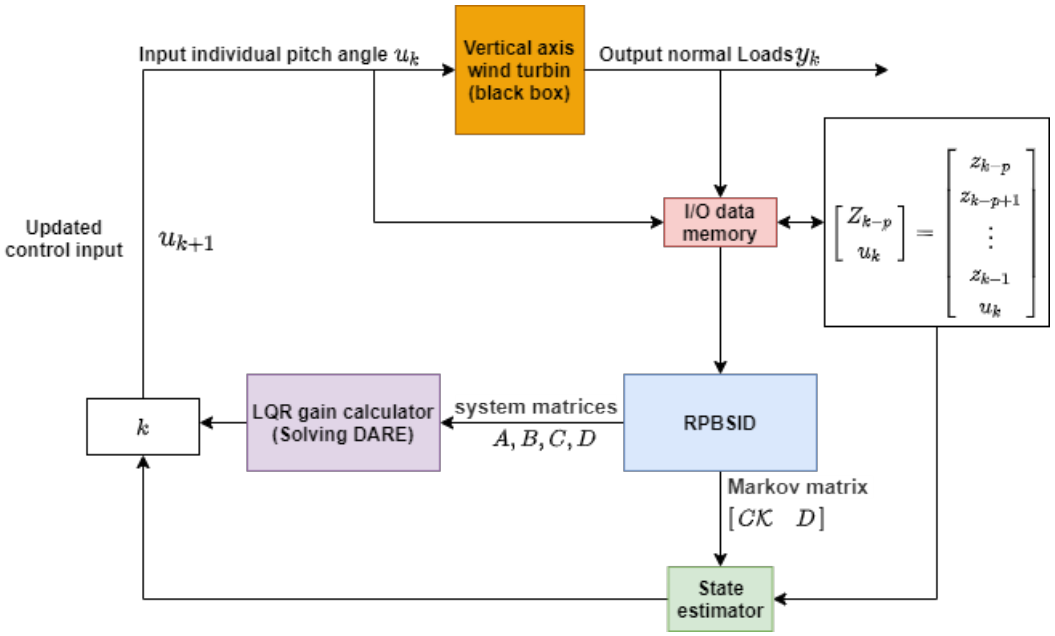

Figure 3-4: Block diagram of the closed-loop system using LQR based SPC

Chapter 4

Results

This chapter presents the results obtained with the Subspace Predictive Control (SPC) framework introduced in chapter 3. The control system is first tested on the Simulink model to verify the feasibility of the theoretical concepts including online recursive identification, Model Predictive Control (MPC) based SPC, and Linear-Quadratic Regulator (LQR) based SPC. After this, the control methods are applied to Qblade.

4-1 Case Study

The Vertical Axis Wind Turbine (VAWT) simulated in the Simulink model and Qblade is based on the two-bladed 1.5 m H-Darrieus VAWT called PitchVAWT, for which the pitch angle of each blade can be controlled individually [9]. The turbine specifications are summarized in table 4-1. Figure 4-1 shows the global coordinate system and the counter-clock wise rotational direction of the presented VAWT. Furthermore, figure 4-2 provides a top view of the turbine, for which it is clear that blade 1 starts at an azimuth angle of 0° and blade 2 starts at an azimuth angle of 180°.

Table 4-1: Vertical axis wind turbine specifications [9]

Parameter	Value
Number of blades (N_b)	2
Span (s)	1.5 m
Diameter (D)	1.5 m
Chord (c)	7.5 $\times 10^{-2}$ m
Blade airfoil	NACA0021
Strut airfoil	NACA0018
Pitch range	$-10°$ - $10°$
Tip-Speed Ratio range	1 - 4.5

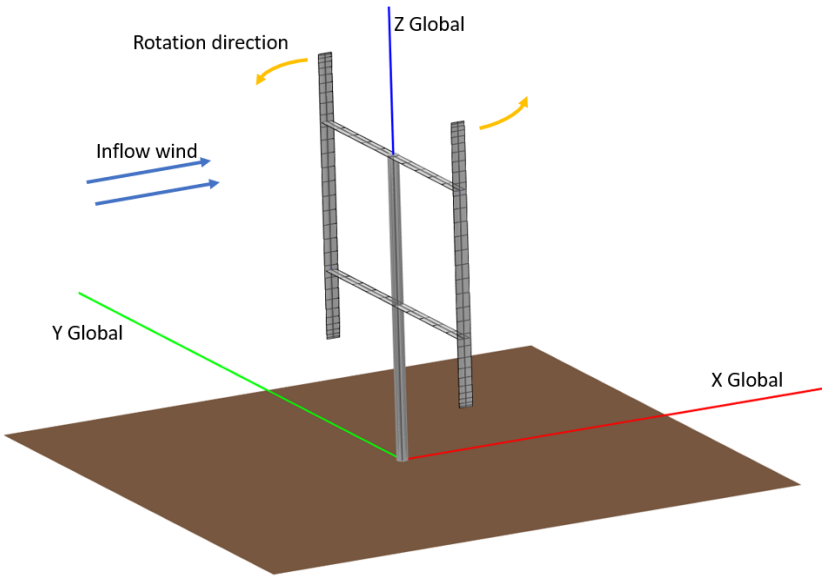

Figure 4-1: The global coordinate system of the two-bladed vertical axis wind turbine adapted from Qblade

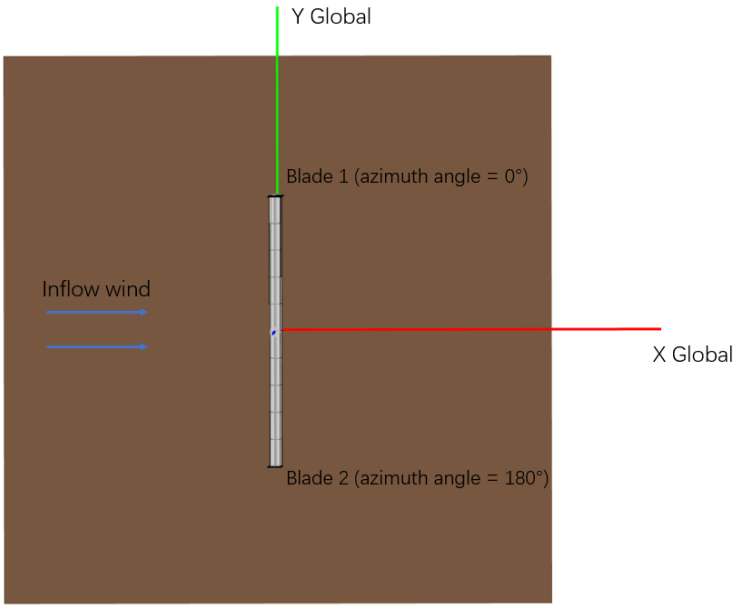

Figure 4-2: Top view of the global coordinate system of the two-bladed vertical axis wind turbine adapted from Qblade

4-2 Simulink Model

The following section presents the normal loads simulated by the Simulink model. Subsequently, the performance of Recursive Predictor-Based Subspace Identification (RPBSID) and the simulation results of applying two control approaches to the Simulink model are presented. Finally, the results are summarized to show the main outcomes of applying MPC based SPC and LQR based SPC.

4-2-1 Model Description

The Simulink model is built according to the method described in section 2-3. The output normal loads of the VAWT system under a constant wind speed of 4 m/s with Tip-Speed Ratio (TSR) of 4.5 and pitch angle of 0 and 5 degrees are shown in figure 4-3. The normal load curve is shifted for blade 1 and blade 2 because the azimuth position of blade 2 is shifted by 180° respected to blade 1. The trend of the normal load is mainly influenced by the Angle of Attack (AOA), which becomes larger at the upstream part and smaller at the downstream part. Furthermore, the positive pitch angle affects the trend and the absolute value of the normal load by moving the load from upwind to downwind, as presented in figure 4-3. The AOA of the blade is reduced by adding a positive pitch according to equation (2-14).

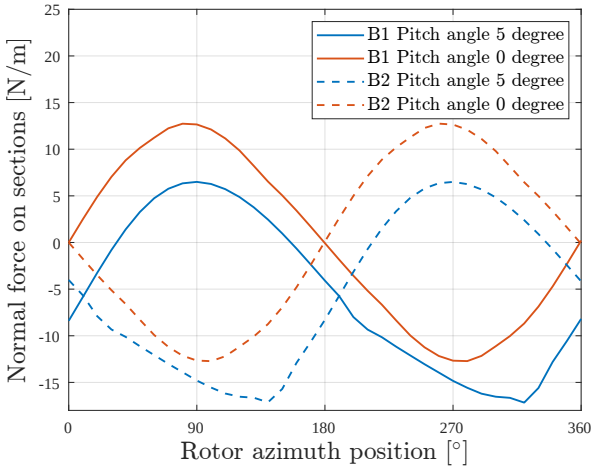

Figure 4-3: Comparison of the normal load obtained with the Simulink model for TSR of 4.5 and for two different pitch angles ($\beta = 0°$ and $\beta = 5°$). The solid line refers to the trend of blade 1 while the dashed line to blade 2

To prove the reliability of the Simulink model, the results for the normal load are compared with the Actuator Cylinder (AC) and Qblade model in figure 4-4. Since Qblade is a 3D model, it is important to note that the normal load is extracted at the mid-section for the comparison. The Simulink model provides an overall similar trend. However, the absolute value of the normal load is different between the Simulink model and the other two aerodynamic models. This is because different models use different methods to compute the relative velocity and AOA at the blade section. As a proof of the concept, the comparison of AOA and relative velocity can be found in figure 4-5 and figure 4-6.

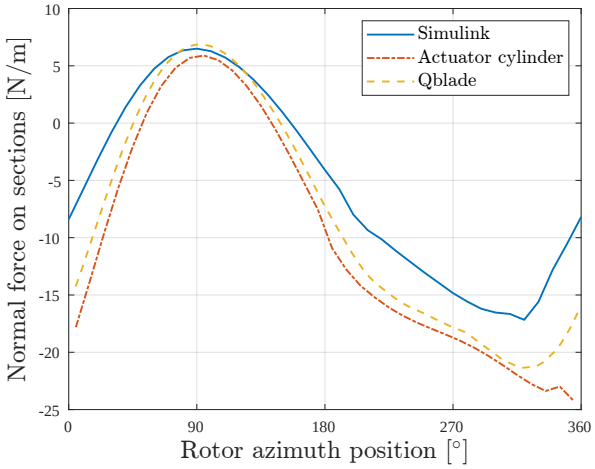

Figure 4-4: Normal forces comparison between Simulink, AC and Qblade model with TSR of 4.5 and pitch angle of 5°

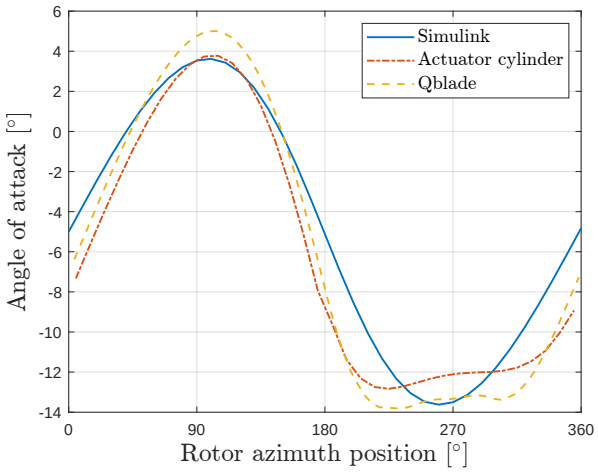

Figure 4-5: Comparison of the angle of attack between Simulink, AC and Qblade model with TSR of 4.5 and pitch angle of 5°

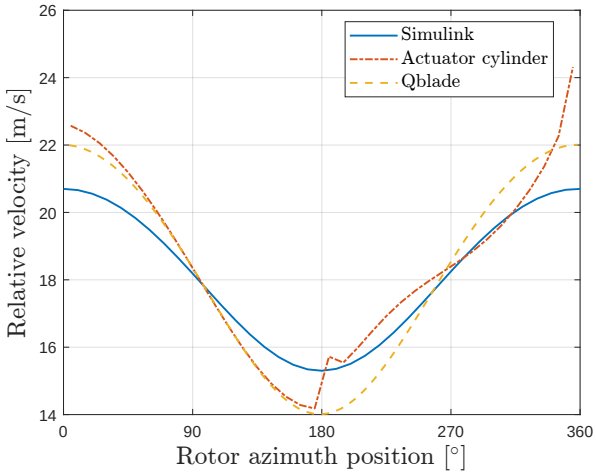

Figure 4-6: Comparison of the relative velocity between Simulink, AC and Qblade model with TSR of 4.5 and pitch angle of 5°

For the Simulink model, the induction factor is assumed to be the same across the rotor plane. Hence, the AOA and relative velocity have a similar trend for the upstream and downstream parts as shown in figure 4-5 and figure 4-6. This causes the main difference between the three models since the actual induction varies with the azimuth position of the rotor. The minimum of the relative velocity occurs at the same rotor azimuth position of 180° for three models because the blade is moving in the same direction of the inflow wind. Further, because of the different model formulations, the optimal operating conditions for power generation are also different. For AC model, the optimal condition is TSR of 4.5 and pitch angle of 5°. For Qblade, it is TSR of 4 and pitch angle of 0°. To be consistent with the Qblade simulation, the baseline condition is chosen as TSR of 4 and pitch angle of 0°.

4-2-2 Online Open-Loop System Identification

Before connecting the controller to the Simulink model, the RPBSID introduced in chapter 3 is applied to test the online identification performance. To identify a system, the input sequence needs to satisfy the persistency of excitation, which means that the input sequence needs to contain enough information in the frequency domain to excite all the modes for the identified model [42]. For this reason, a Pseudo-Random Binary Sequence (PRBS) is used as the pitch signal to excite the VAWT model. The first 0.5 seconds of the input PRBS is shown in figure 4-7.

The identified system order also needs to be defined. As discussed in chapter 3, the order of the identified system can be determined by checking the singular value of the estimated state sequence [42]. The resulted singular values are shown in figure 4-8 in a log scale. It can be seen from the figure that there is a big gap at order 2, 4, 6, 8 and 10. A choice of a larger system order often yields to heavier computational load. But, a choice of a small system order may result in a bad identification performance because not all the dynamics of the system are considered. For our application, the computational load is not significant. Hence, a system order of 10 is decided because a lower system order fails to fully represent the system dynamics.

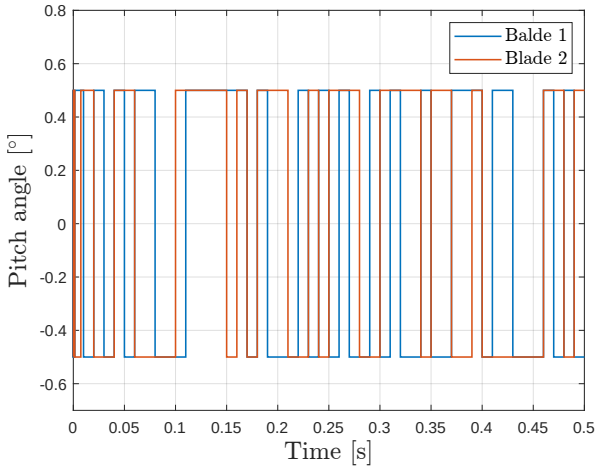

Figure 4-7: Pseudo-random binary pitch signal for persistent excitation (zoom in to first 0.5 s)

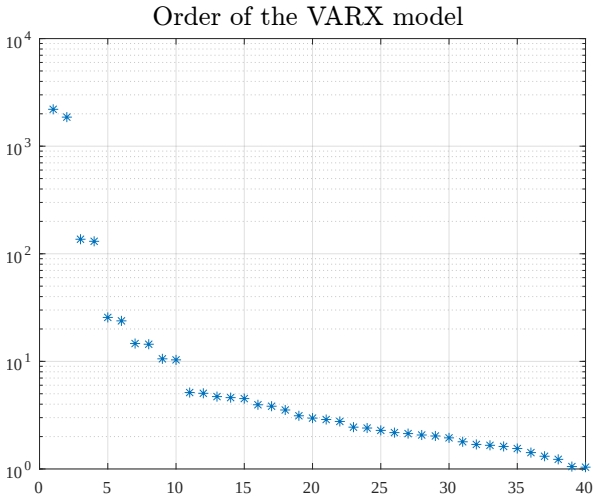

Figure 4-8: Singular values of the estimated state sequence under the pseudo-random binary pitch excitation

Further, the RPBSID as discussed in section 3-1-4 is applied to the Simulink model. As a trade-off between the computational load and the identification performance, the past window size of RPBSID is chosen as 30 which covers one period of rotation (0.2945 s). The forgetting factor denotes how fast the old data is discarded. For a steady-state with no dynamics change in the system, the forgetting factor can be chosen as 1 to keep collecting the Inuput/Output (I/O) information. To adapt to the varying dynamics and guarantee the robustness of the identification, a forgetting factor of 0.995 is applied in this thesis [52]. The result of the online system identification under a constant, steady wind speed of 4 m/s is shown in figure 4-9.

The simulation time is set as 30 s to obtain enough I/O data for the identification. The

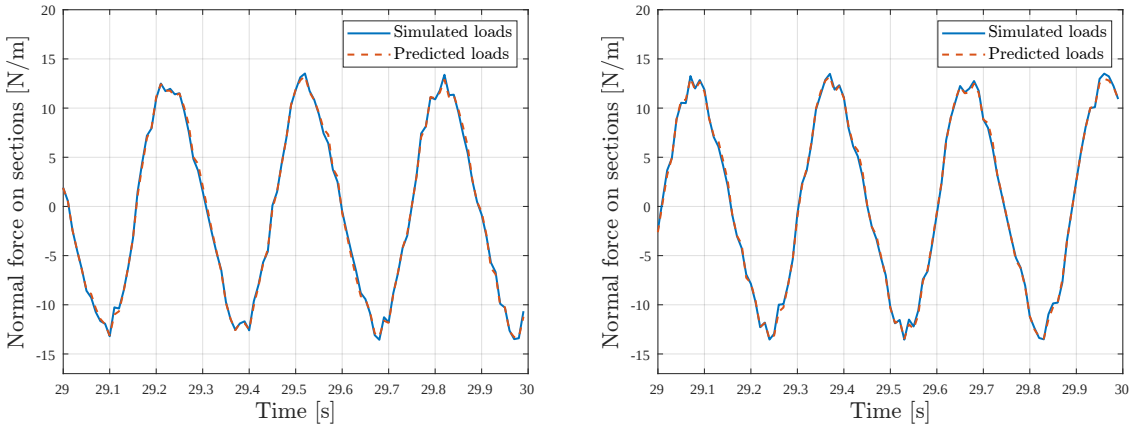

(a) Blade 1 **(b)** Blade 2

Figure 4-9: One-step predicted response comparison under a constant wind speed of 4 m/s and a pseudo-random binary pitch signal for blade 1 (a) and for blade 2 (b)

Normalized Root Mean Squared Error (NRMSE) fitness values of one-step prediction are 97.02% and 96.86% for blade 1 and blade 2. Here, the identification result has a bias of 0.16% for blade 1 and blade 2. The biased estimated model is expected since the past window size is finite [45, 46]. Also, the effect of a finite window size is hard to quantify, and the interested readers are referred to [45, 46]. However, the small bias is negligible for the control design.

To test the adaptive nature of the online identification method, the wind speed is set to a step signal changing from 4 m/s to 5 m/s at 15 s. The pitch signal of the system is kept as the PRBS to satisfy the persistency of excitation. Figure 4-10 shows the change of the normal loads under a step wind.

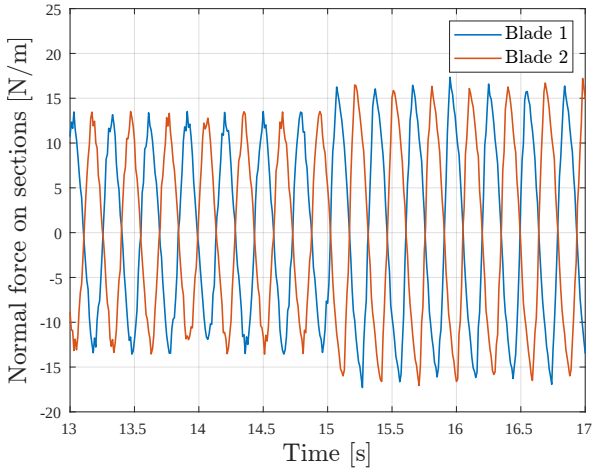

Figure 4-10: Output normal loads for blade 1 and blade 2 of the Simulink model under a step wind changing from 4 m/s to 5 m/s at 15 s

After running the online recursive identification method, the one-step predicted outputs of the identified system at high wind speed 5 m/s is compared to the simulated outputs as shown

in figure 4-11. The one-step prediction shows a larger bias of 2.48% and a lower NRMSE fitness of 91.30% and 89.04% for blade 1 and blade 2 compared to constant wind speed case. Under the same past window size, forgetting factor and simulation time, the identification performance under a step wind is weaker than under a steady wind because of the changing operating condition. However, the identified model is sufficient for the control design. This also shows the RPBSID method can respond to the time-varying dynamics of the system and update the identified model accordingly.

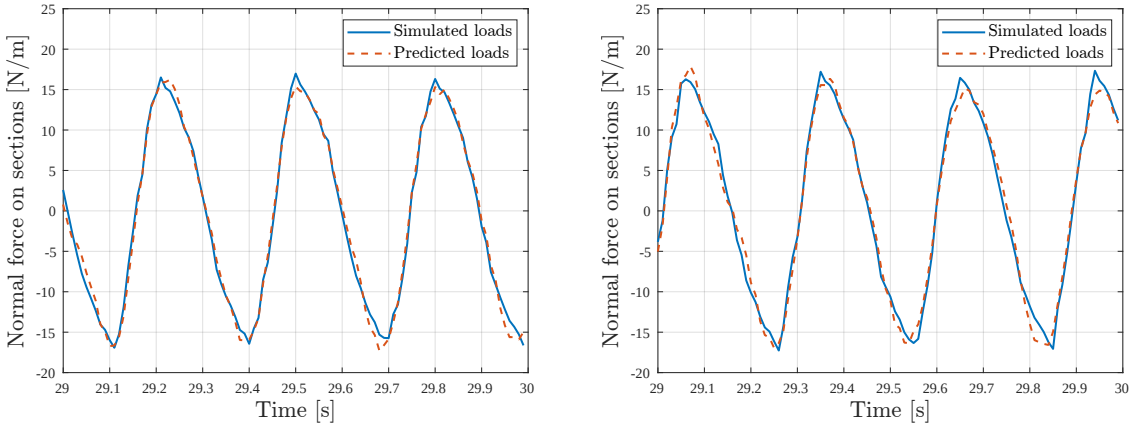

(a) Blade 1 **(b)** Blade 2

Figure 4-11: One-step predicted response comparison under a stepwise wind speed changing from 4 m/s to 5 m/s at 15 s and a pseudo-random binary pitch signal for blade 1 (a) and for blade 2 (b)

4-2-3 Online Closed-Loop Individual Pitch Control

As described in chapter 3, two methods will be applied to solve the blade loads mitigation problem. Both MPC and LQR are based on the RPBSID method tested in section 4-2-2. For both approaches, the controller is first switched off to make sure there is enough information collected for the system identification. Hence, the controller is designed as a time-triggered block. The time of the open-loop identification is set to 10 s to acquire a desirable identified model before applying any control action. After the controller is switched on, the online recursive identification is activated in a closed-loop to update the estimated model responding to the dynamics change in the VAWT system (i.e., dynamics change caused by a varying wind speed). To test the MPC based SPC, the wind speed is set as a step signal increase from 4 m/s to 5 m/s at 40 s. This simulation time is chosen based on the convergence speed of the MPC based SPC. The closed-loop VAWT simulation also includes some process noise (i.e., some uncontrolled input disturbance) for the robust test and a more realistic scenario.

To calculate the optimal pitch trajectory using the MPC based SPC introduced in section 3-4, the weighting matrices of the cost function need to be decided first. The weighting matrices used in this thesis are set to $Q_m = I$ and $R_m = 5I$. For a step wind changes at time 40 s, the control inputs for blade 1 and blade 2 also change adaptively as shown in figure 4-12.

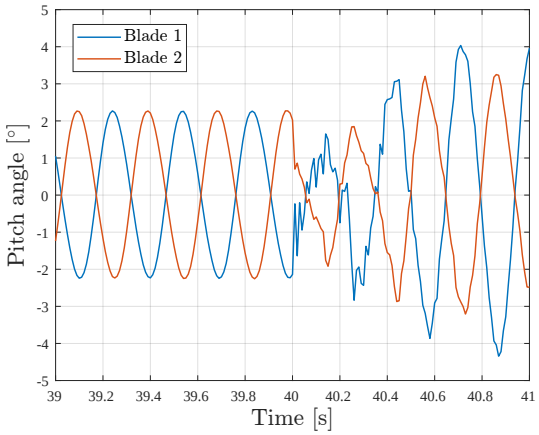

(a) Controlled pitch trajectory

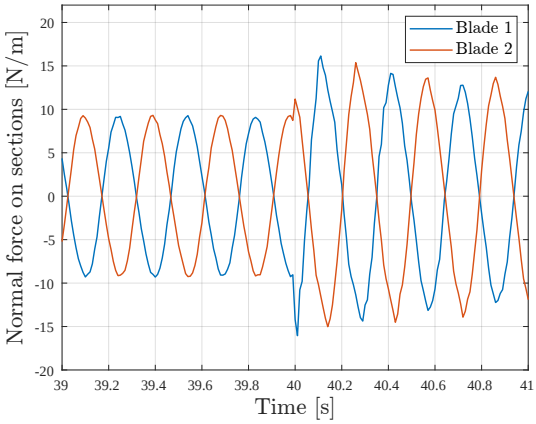

(b) Controlled normal load

Figure 4-12: Closed-loop simulation result using MPC based SPC when wind speed changes from 4 m/s to 5 m/s at 40 s

In figure 4-12a, the amplitude of the controlled pitch trajectory increases after the wind speed changes. However, it can be seen that the pitch trajectory is not stable. This is because the closed-loop data-driven control system needs time to adapt to the changing operating condition and acquire a stable pitch trajectory.

In figure 4-13 and 4-14, the converged pitch trajectory and the corresponding load reduction results are shown as a function of the rotor azimuth position. This is because the normal load and the controlled pitch show a similar trend for each rotation after convergence. By showing the results during one rotation, the details of the plots are more clearly presented.

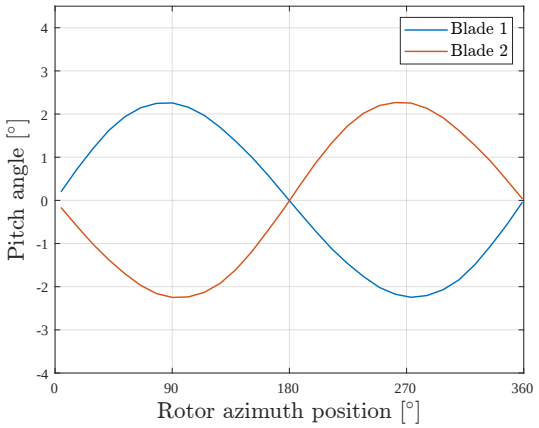

(a) Under the wind speed of 4 m/s

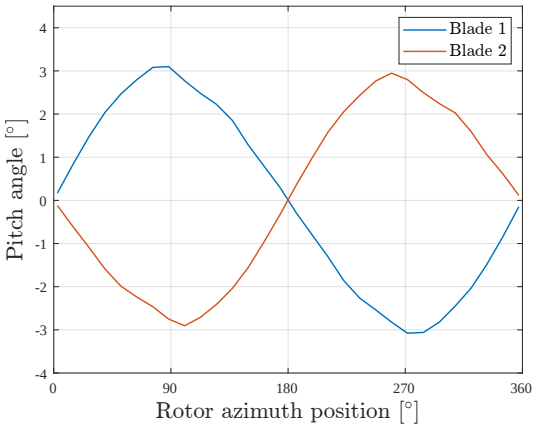

(b) Under the wind speed of 5 m/s

Figure 4-13: Controlled pitch trajectory of the MPC based SPC method

The amplitude of the pitch trajectory increases from 2.2° to 3.0° adaptively when the wind speed rises from 4 m/s to 5 m/s to maintain the load reduction performance. For simplicity and clarity, the results are only plotted for blade 1 because blade 2 shows a similar trend.

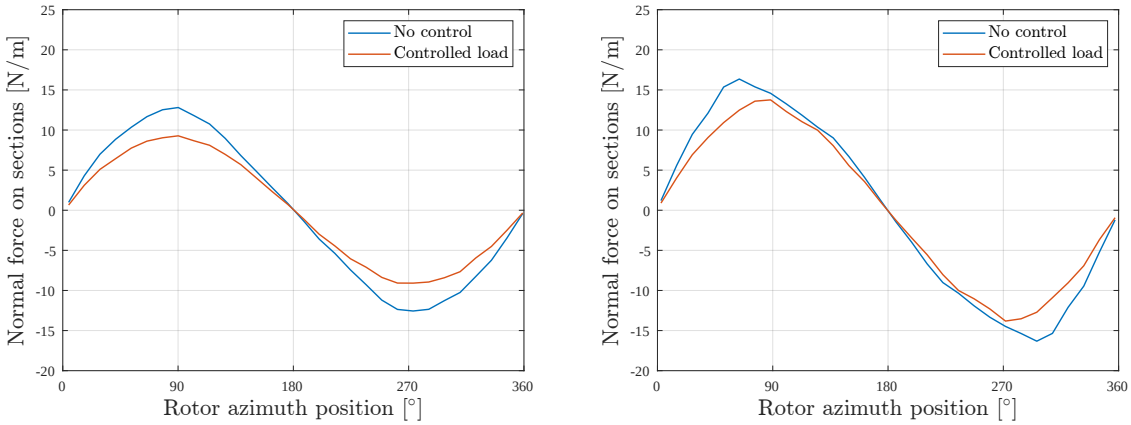

(a) Controlled normal load under the wind speed of 4 m/s **(b)** Controlled normal load under the wind speed of 5 m/s

Figure 4-14: Control result of the MPC based SPC method for blade 1

The resulting absolute value reduction ratio of the normal load for blade 1 is 28.53 % under the wind speed of 4 m/s, and 15.61 % under the wind speed of 5 m/s. Because the weighting matrices are kept the same under a higher wind speed and the total normal load increases, the induction ratio decreases. To keep the same reduction ratio, the weighting matrix Q_m needs to be set larger to obtain a greater penalization on the normal load.

The power spectra of the normal load are shown in figure 4-15. It can be found that most power is located at 1P frequency, which corresponds to 3.4 Hz. The power spectra have some high-frequency content because white noise is added to the input signal when running the simulation. According to figure 4-15, the power of the normal load for 1P frequency is significantly reduced. For 1P frequency, the normal load power is reduced by 40.91 % under the wind speed of 4 m/s and 27.49% under the wind speed of 5 m/s. The difference in the load reduction is caused by the fixed weighting matrices as discussed before.

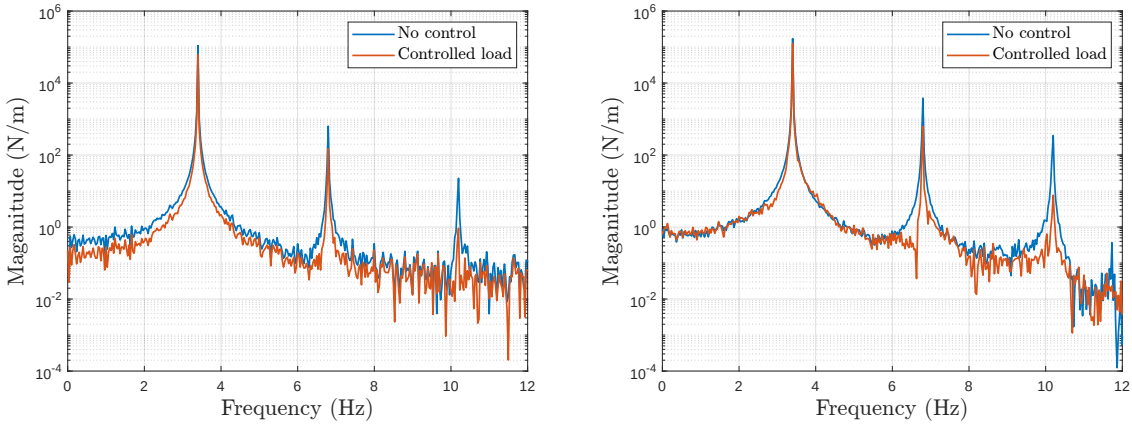

Figure 4-15: Blade 1 normal load power spectrum comparison of the MPC based SPC approach under the wind speed of 4 m/s (left) and 5 m/s (right)

These results show that the individual pitch controller using MPC based SPC achieves a reduction above 27.49% in the 1P component of the load. The MPC based SPC method also shows the potential of automatically adapting to the time-varying dynamics in the system and adjusting the control input to keep the optimal trade-off between pitch actuation and normal load reduction.

The second approach is the LQR based SPC as discussed in section 3-5. The weighting matrices Q_l and R_l are set as the identity matrix with the power of 1 and 20 to penalize the input and system state respectively. To guarantee the stability of the closed-loop system, a higher forgetting factor of 0.9999 is used. To obtain a more accurate identified system before the controller is applied, the open-loop identification is extended from 10 s to 30 s compared to the MPC based SPC case. Then, the wind speed is set as a step signal increases from 4 m/s to 5 m/s at 60 s. In this way, the closed-loop simulation time is 30 s (wind step time minus open-loop identification time), which is the same as the MPC based SPC case.

Similar to the MPC based SPC case, the controlled pitch trajectory responses to the step wind speed as shown in figure 4-16. Because the LQR control gain is updated at a slow rate as defined in equation 3-35, the pitch trajectory is less disturbed compared to the SPC case when the wind speed changes.

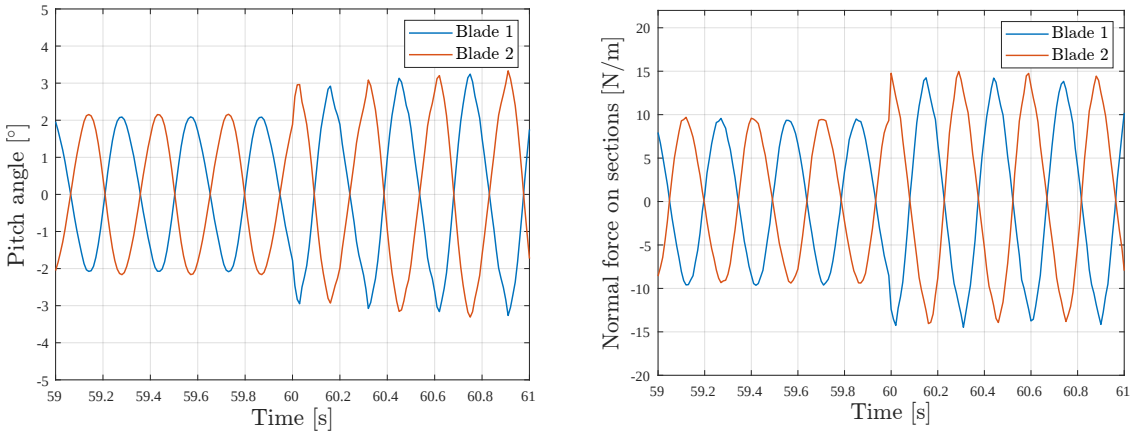

(a) Controlled pitch trajectory

(b) Controlled normal load

Figure 4-16: Closed-loop simulation result using LQR based SPC when wind speed changes from 4 m/s to 5 m/s at 60 s

The converged pitch trajectory and the corresponding load reduction result are shown in figure 4-17 and figure 4-18. The controlled pitch trajectory is similar to the one of MPC based SPC because both of them are calculated based on the model identified by RPBSID algorithm. The peak absolute value of the normal load is reduced by 25.93 % under the wind speed of 4 m/s, and 15.75 % under the wind speed of 5 m/s. The power spectra of the normal load are shown in figure 4-19. By applying the LQR based SPC, the normal load power of 1P frequency is reduced by 41.02% under the wind speed of 4 m/s, and 27.54% under the wind speed of 5 m/s.

Like the MPC based SPC, the LQR based SPC also successfully reduced the normal load on

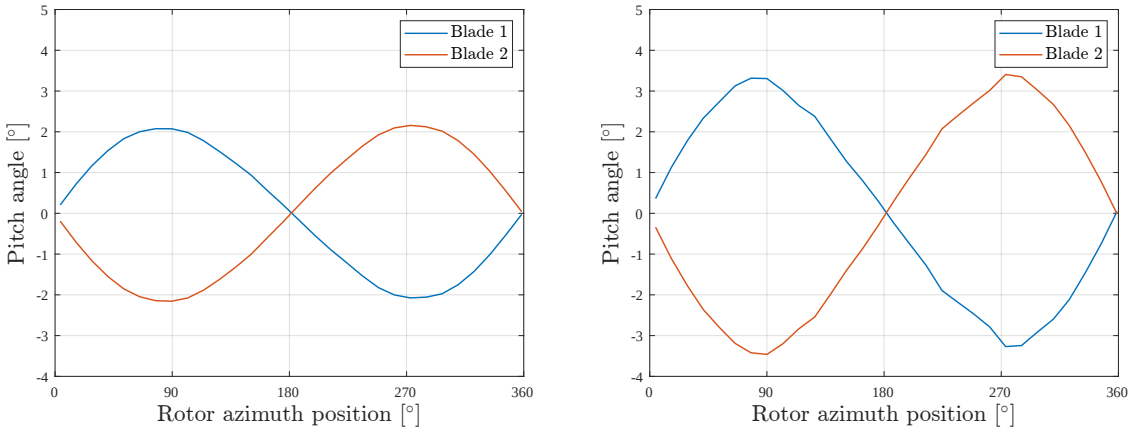

(a) Under the wind speed of 4 m/s **(b)** Under the wind speed of 5 m/s

Figure 4-17: Controlled pitch trajectory of the LQR based SPC method

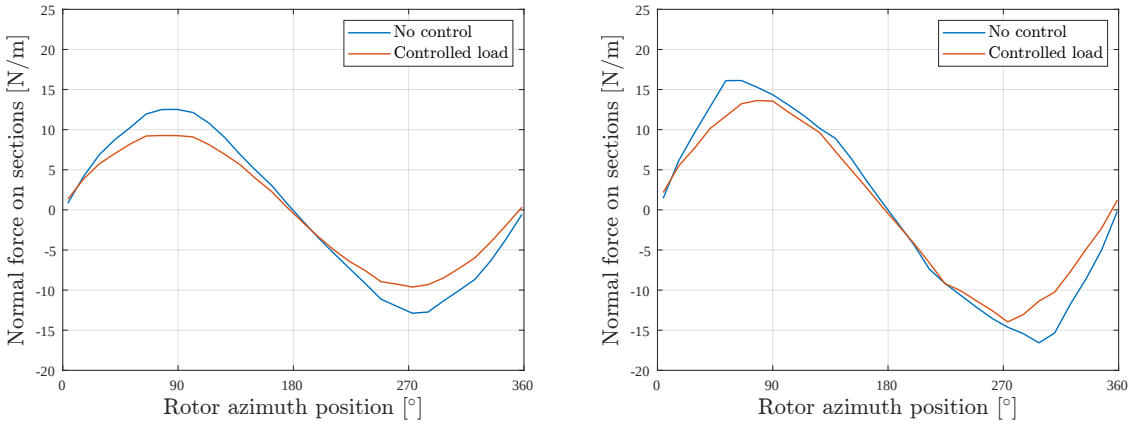

(a) Controlled normal load under the wind speed of 4 m/s **(b)** Controlled normal load under the wind speed of 5 m/s

Figure 4-18: Control result of the LQR based SPC method for blade 1

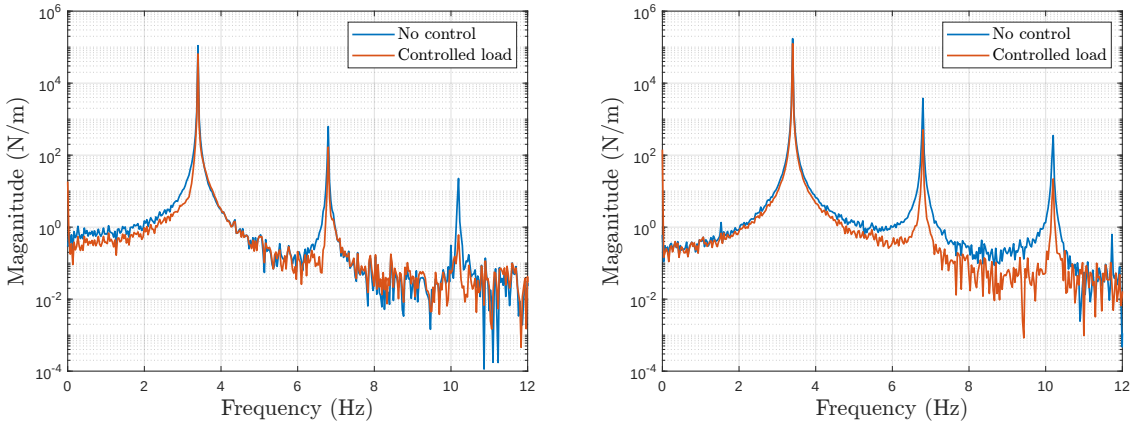

Figure 4-19: Blade 1 normal load power spectrum comparison of the LQR based SPC approach under the wind speed of 4 m/s (left) and 5 m/s (right)

the blades. However, the quantitative results are not compared because the penalization term is different for MPC and LQR. Both methods can achieve a similar load reduction by tuning the weighting matrices. However, during the case study, there are some findings related to the implementation of the MPC and LQR methods, which are worth discussing.

First, the LQR has more parameters to tune such as the factor a and b defined in equation 3-35. Further, the LQR requires more computational efforts in the identification part since the system matrix A, B, C, and D need to be identified. Also, it is found that a larger forgetting factor needs to be set to guarantee the stability of LQR. Besides, the input pitch signal may exceed the design limit because the LQR solves an unconstrained optimization problem. Because of these reasons, the MPC based SPC is chosen for the VAWT application and further validated in Qblade. It is easy to implement, with more robust performance and minimum identification computational cost.

4-3 Qblade Results

Through the tests presented in section 4-2, the MPC based SPC shows a good load reduction performance and easier implementation compared to LQR based SPC. In this section, to apply the MPC based SPC in a more realistic scenario, Qblade is used. The results are presented in the following sections.

4-3-1 Online Open-Loop System Identification

For the closed-loop control system, the normal load of each blade should be provided by the Qblade simulation as a feedback signal. However, for the Bladed format used to compile the controller, the normal load is not provided in the communication data array because Bladed is created for Horizontal Axis Wind Turbine (HAWT)s [53]. Only the bending moments are available since it is often used for the load reduction control for HAWTs [8]. Hence, the MPC based SPC is separated into two parts. The RPBSID is first used to estimate the dynamic model of the VAWT based on the I/O data simulated by Qblade. Then, the optimal pitch trajectory is calculated based on the identified VAWT model. Further, it is used in Qblade as a feedforward pitch signal to validate the control performance. Besides the pitch controller, a TSR tracker is implemented to regulate the generator speed [54]. The TSR is kept as 4 to obtain the maximum power generation. The proportional gain and integral gain of the TSR tracker are tuned as -10 and -0.5 for good control performance. The value of the TSR tracker gain is provided by the author's daily supervisor.

In order to conduct the RPBSID method on the open-loop VAWT system, the I/O data need to be collected through the Qblade simulation. In section 4-1-2, a PRBS is used as the excitation pitch signal for the Simulink model. For a more realistic scenario, a PRBS is not suitable because it contains extremely high-frequency components. To avoid this situation, the individual pitch angle is set to a sweep signal in order to satisfy the persistent excitation condition. To choose a suitable sweep frequency, the power spectrum of the Qblade simulated normal loads under a uniform wind speed of 4 m/s is checked as shown in figure 4-20. It can

be found that the power of the normal load is mainly located at 1P frequency (3.4 Hz), with some low-value components at 2P and 3P frequency (6.8 Hz and 10.2 Hz). Hence, the initial sweep frequency is set as 0.5 and the final sweep frequency is set as 7 to cover the 1P and 2P frequency of the VAWT model.

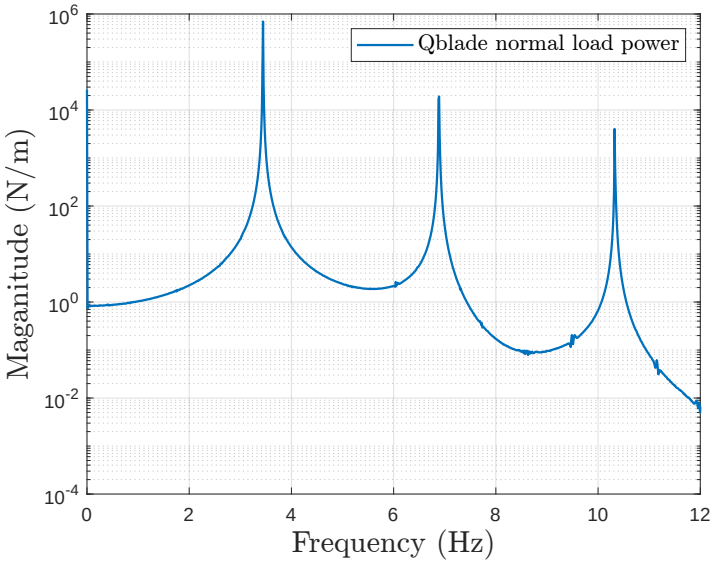

Figure 4-20: Power spectrum of Qblade normal load output with zero pitch angle (TSR: 4 Steady wind speed: 4 m/s)

The open-loop identification is conducted for both uniform wind and turbulent wind cases. To get a more accurate result, the sample time of Qblade (0.003588 s) is set smaller than the sample time of the Simulink model (0.01 s). Hence, the past window size of the identification is first set to a larger value of 80 to cover one period of rotation (0.2945 s). However, a larger window size results in an algorithm with linear increased computational load [43]. Hence, the past window size is reduced to 30 which is sufficient to capture the system dynamics with a good identification result. The system order is set to 10 after checking the singular values. The forgetting factor is first set to 1 to guarantee the stability of the RPBSID algorithm. Under a uniform wind of 4 m/s, the result of the online system identification is shown in figure 4-21. The simulation duration is set to 50 s to guarantee that enough data is collected for the identification. The values of NRMSE fitness of one-step prediction are 96.59% and 97.05% for blade 1 and blade 2. Furthermore, a forgetting factor of 0.9999 is applied to test the robustness of the RPBSID. The identification result is shown in figure 4-22. The identification performance weakened with respect to the case with forgetting factor 1 because of a lower forgetting factor. However, the resulting NRMSE fitness values are still desirable as 89.01% and 86.39% for blade 1 and blade 2.

For the turbulent wind case, the wind profile is shown in figure 4-23. The turbulent wind field with a mean wind speed of 4 m/s and 5% Turbulence Intensity (TI) is generated with TurbSim model [55]. The mean wind speed is set to be the same as the uniform wind case, and the TI is chosen within a commonly encountered range at the North Sea [56]. To acquire a valid identified VAWT system, more I/O data is used to train the RPBSID than the uniform

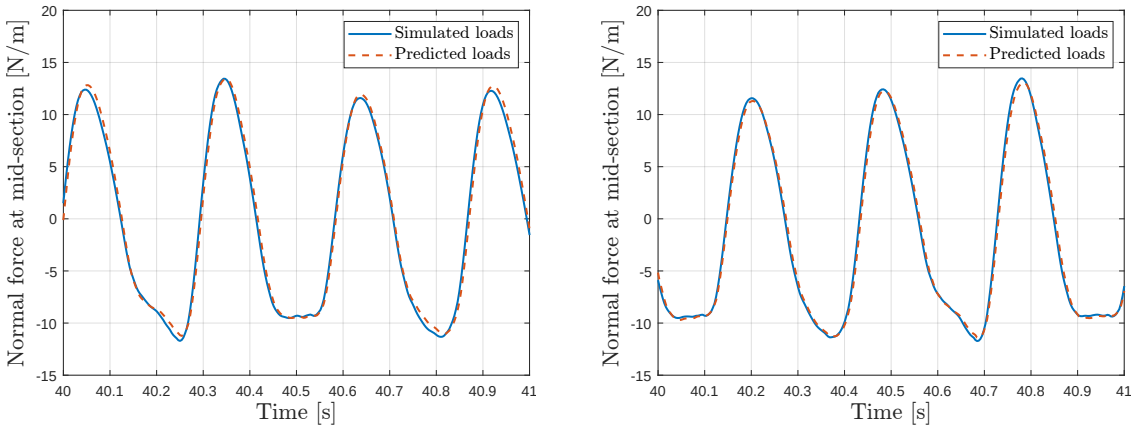

(a) Blade 1 **(b)** Blade 2

Figure 4-21: One-step predicted response comparison under a uniform wind speed of 4 m/s with the forgetting factor of 1 for blade 1 (a) and blade 2 (b)

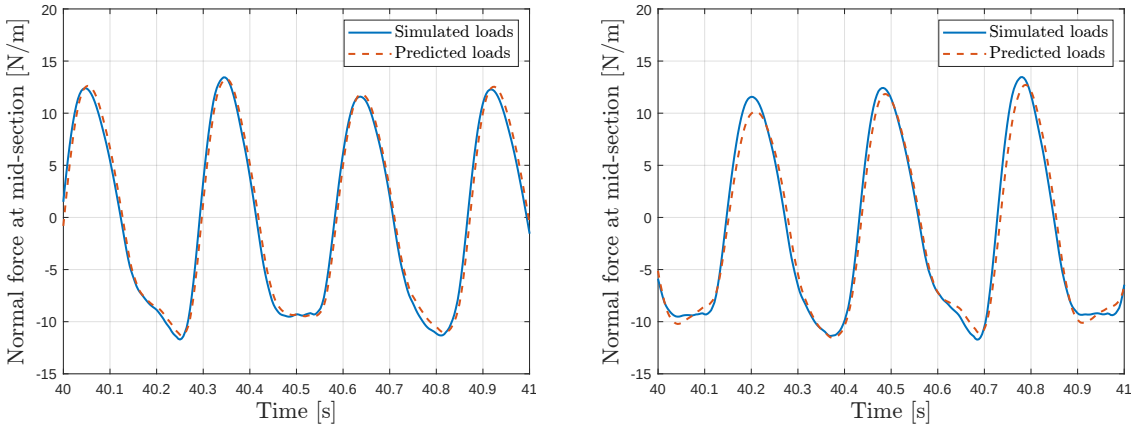

(a) Blade 1 **(b)** Blade 2

Figure 4-22: One-step predicted response comparison under a uniform wind speed of 4 m/s with the forgetting factor of 0.9999 for blade 1 (a) and blade 2 (b)

wind case. Running RPBSID for 100s with the forgetting factor of 1, the identification results are show in 4-24. The values of NRMSE fitness of one-step prediction are 93.65% and 92.58% for blade 1 and blade 2. However, under a turbulent wind, the identification result is more sensitive to the forgetting factor because the turbulent wind causes a less stable operating condition. Compared to the uniform wind case, the identification results of a forgetting factor of 0.9999 has a larger bias and do not correctly predict the normal load of blade 2 which are shown in figure 4-25.

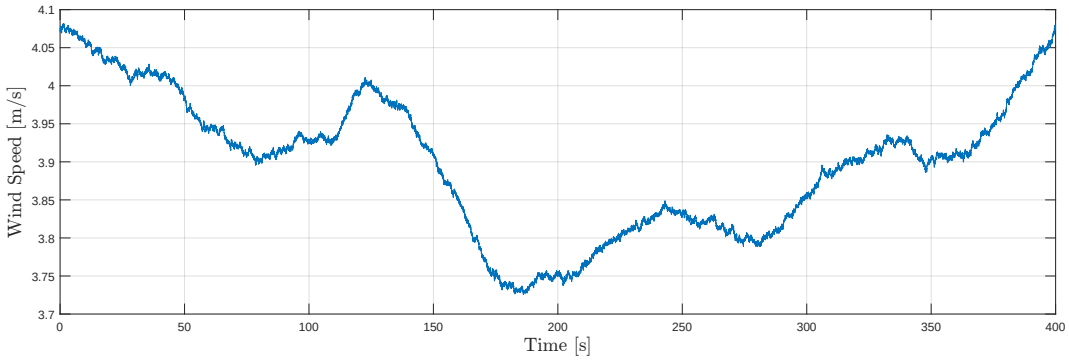

Figure 4-23: Turbulent wind field with a mean wind speed of 4 m/s and 5% TI

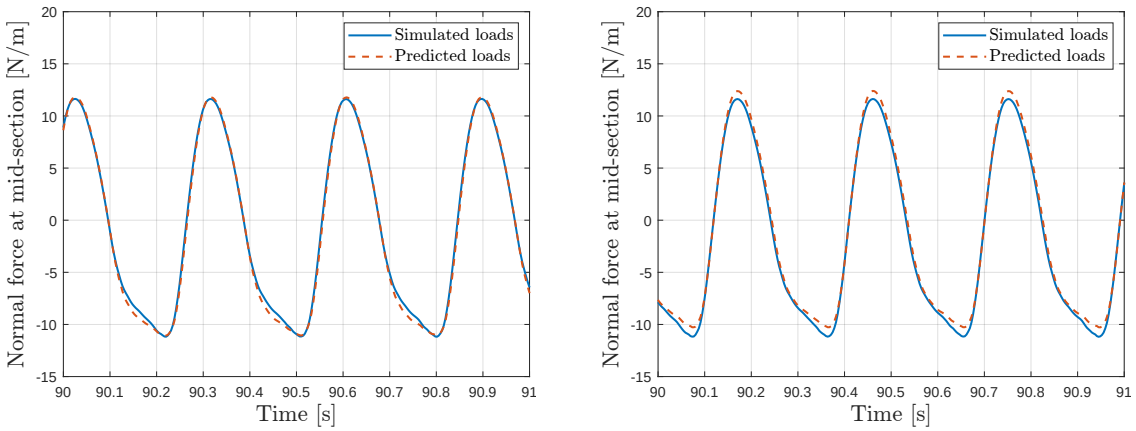

(a) Blade 1 **(b)** Blade 2

Figure 4-24: One-step predicted response comparison under a turbulent wind field with a mean wind speed of 4 m/s and 5% TI with the forgetting factor of 1 for blade 1 (a) and blade 2 (b)

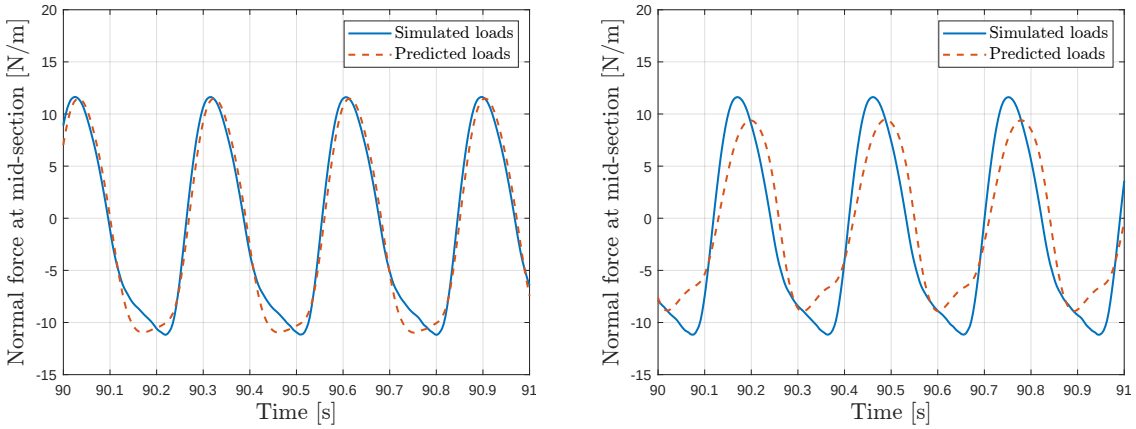

(a) Blade 1 **(b)** Blade 2

Figure 4-25: One-step predicted response comparison under a turbulent wind field with a mean wind speed of 4 m/s and 5% TI with the forgetting factor of 0.9999 for blade 1 (a) and blade 2 (b)

4-3-2 Offline Individual Pitch Control

The optimal pitch trajectory is calculated based on the model identified in section 4-3-1. To use the pitch trajectory as a control signal, it is defined as a function of the blade azimuth angle. The azimuth position of the rotor is available in the data exchange channel, which denotes the azimuth position of blade 1. To acquire the azimuth position of blade 2, a phase shift of 180° is added. Based on the azimuth position of each blade, the desired pitch angle can be calculated according to the optimal pitch trajectory. The optimal pitch trajectory is calculated based on the open-loop identification conducted in section 4-3-1.

For the uniform wind case, the optimal pitch trajectory is shown in figure 4-26a with an amplitude of 2.65°, and the normal load reduction performance is shown in figure 4-26b. The absolute value of the normal load is reduced by 18.02% for the upwind peak and 13.45% for the downwind trend. The power spectrum comparison is shown in figure 4-27 where the power of the normal load is reduced at 1P, 2P and 3P frequency. Since most normal load power locates at 1P frequency, the power reduction ratio is calculated for 1P frequency as 30.34%.

For the turbulent wind case, the optimal pitch trajectory is shown in figure 4-28a. The amplitude of the optimal pitch trajectory is 3.16° which is larger than the one of the uniform wind case due to a different identified model. The controlled normal load is shown in figure 4-28b. The absolute value of the normal load is reduced by 22.52% in the upwind peak and 16.67% in the downwind trend. The power spectrum comparison is shown in figure 4-29. Different from the uniform wind case, the power spectrum shown in figure 4-29 is noisier and has some high frequency components because of the turbulent wind. For 1P frequency, the power of the normal load is reduced by 38.40%. In both wind cases, the results show a good normal load reduction performance using the optimal pitch trajectory. However, the pitch actuation used to reduce the normal load also causes a drop in the power coefficient, as shown in figure 4-30.

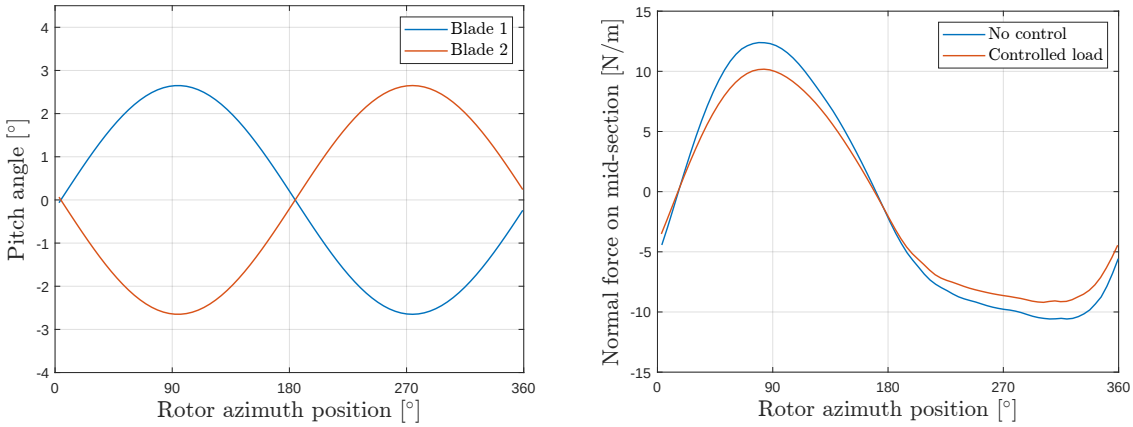

(a) Optimal pitch trajectory **(b)** Controlled normal load

Figure 4-26: Control result of the offline individual pitch control under a uniform wind of 4 m/s

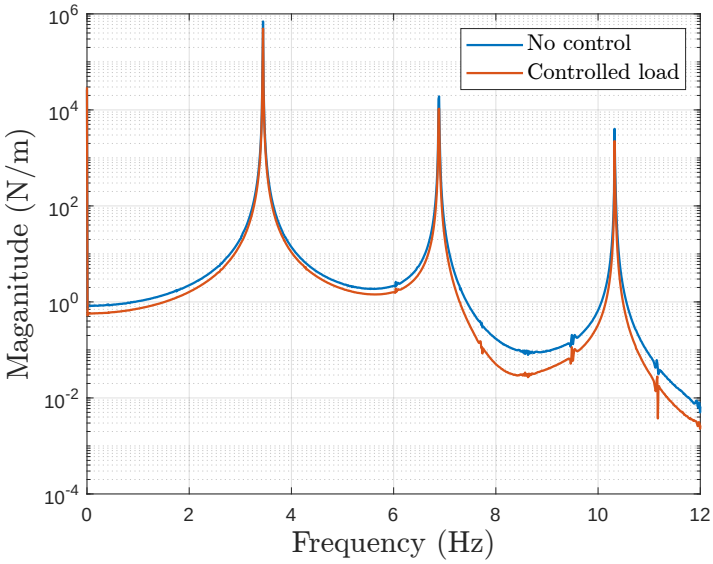

Figure 4-27: Normal load power spectrum comparison of the offline individual pitch control under a uniform wind of 4 m/s

With a pitch trajectory increased from 2.65° to 3.16°, the power coefficient drops 25% more. This power coefficient reduction is expected because when the pitch actuation is applied, the turbine no longer works at the optimal condition for power generation. Hence, the larger the pitch actuation is, the turbine works further away from the optimal condition, and the power coefficient drops more. It is already found for HAWTs that the load reduction and the power maximization are two conflicting objectives [44]. This can also be extended to the VAWTs. To summarize, when using pitch control to reduce the load on the VAWT, the power coefficient is an important trade-off to be considered.

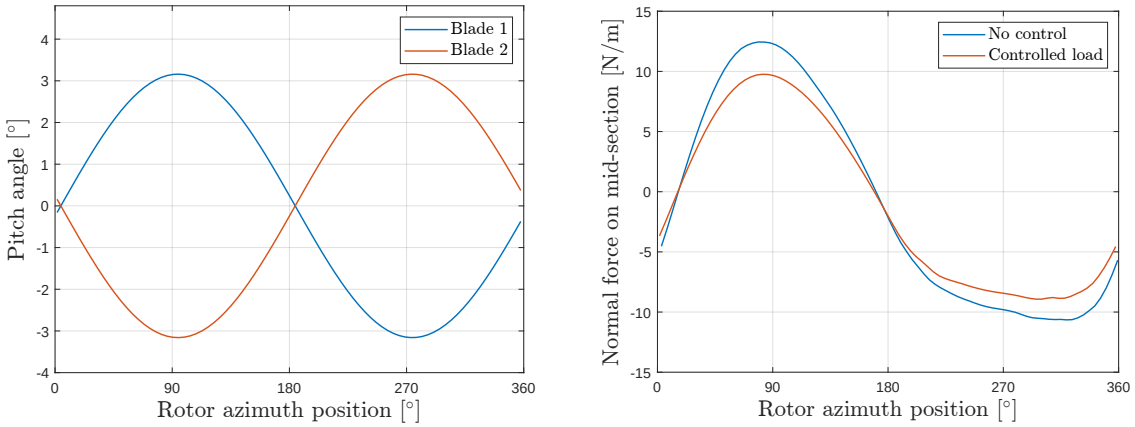

(a) Optimal pitch trajectory **(b)** Controlled normal load

Figure 4-28: Control result of the offline individual pitch control under a turbulent wind field with a mean wind speed of 4 m/s and 5% TI

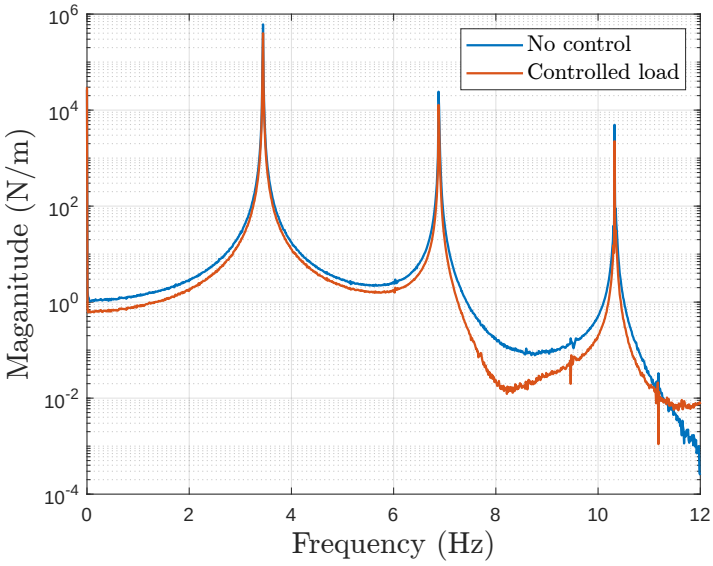

Figure 4-29: Normal load power spectrum comparison of the offline individual pitch control under a turbulent wind field with a mean wind speed of 4 m/s and 5% TI

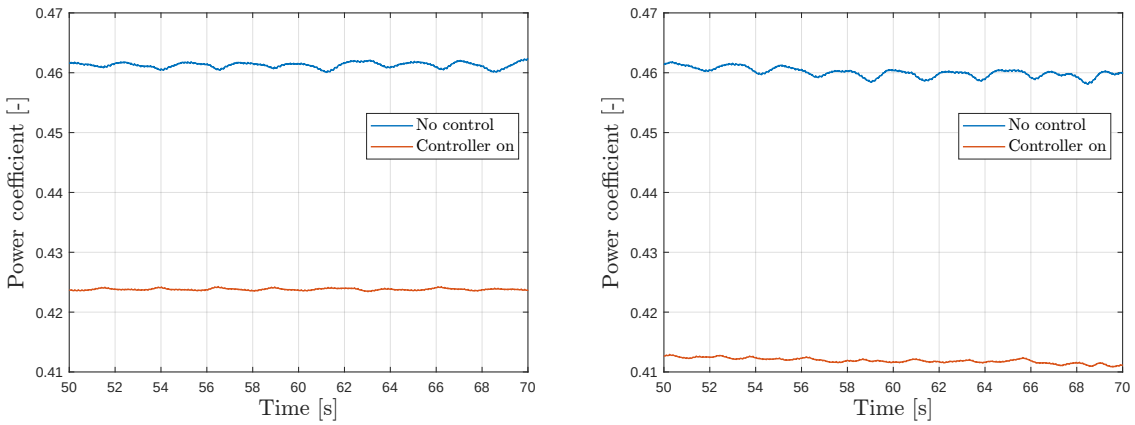

(a) Wind speed 4 m/s

(b) Mean wind speed 4 m/s TI: 5%

Figure 4-30: Power coefficient comparison for uniform wind case (a) and turbulent wind case (b) using the optimal pitch trajectories with the amplitude of 2.65° (a) and 3.16° (b)

Chapter 5

Conclusions and Future Recommendations

5-1 Conclusions

The Subspace Predictive Control (SPC) presented in this thesis shows the potential of reducing the blade loads of the Vertical Axis Wind Turbine (VAWT). For the thesis objectives presented in chapter 1, the answers have been found as:

- ***Designing a closed-loop control system that reduces the blade loads on a VAWT under variable operating conditions***. The system dynamics are identified by the subspace identification method under a persistent excitation signal. Further, the Recursive Least Square (RLS) method is used to achieve the online identification that can capture the time-varying dynamics of the VAWT system. The Recursive Predictor-Based Subspace Identification (RPBSID) applied ensures the closed-loop control system can work in different operating conditions, such as a step in wind speed. The Model Predictive Control (MPC) based SPC and Linear-Quadratic Regulator (LQR) based SPC are then designed to close the control loop. The results presented in chapter 4 show that a significant load reduction is achieved by applying both methods. However, compared to the LQR based SPC, the MPC based SPC is easier to implement with a minimal identification computational effort and a more robust performance. Also, through the case study, it is found that the stability of the close-loop data-driven control is very hard to ensure, especially for the LQR based SPC. This poses an open question for future study.
- ***Proving the feasibility of the individual pitch control system for VAWT on a mid-fidelity software Qblade***. Following the MPC based SPC framework, the open-loop identification using RPBSID is conducted using the I/O data from the Qblade simulation. Further, the supervisory individual pitch controller is connected to the Qblade through a Bladed format. As presented in section 4-3, the optimal pitch trajectory calculated from the identified model significantly reduces the blade loads of the

VAWT in both uniform and turbulent wind conditions. However, the pitch actuation also influences the power coefficient. To achieve a better load reduction, a larger pitch actuation is needed. This will result in a lower power coefficient. Hence, the power coefficient is an important trade-off when applying the pitch control for load reduction.

5-2 Future Recommendations

This thesis explores the potential of applying the active pitch control to reduce the load on the VAWT. The MPC based SPC method applied shows great results in solving the load mitigation problem of VAWTs. To further explore the pitch controller of VAWTs and the data-driven method, there are several future recommendations listed as:

- In this thesis, the rotor speed is assumed as a constant and operates at the best condition for power generation. The rotor speed is regulated by a separate torque controller. Hence, the power production of VAWT is not considered an objective in the MPC cost function. However, the pitch angle also influences power generation. To make a better trade-off between power capture and load reduction for the individual pitch control, the instantaneous power coefficient should also be included in the objective function.
- In section 4-3, Qblade is used to acquire a more realistic result of load reduction performance. However, the pitch controller is not operated in an online closed-loop structure because of the limitations of Qblade. In the future, as Qblade develops, there will be more channels available for the external controller. In this case, the SPC framework can be tested in a closed-loop system.
- The work presented in this thesis ignores some of the realistic factors such as pitch actuation load and pitch actuation frequency. To further build a pitch controller that can be used for a real VAWT, the pitch rate would need to be constrained, and the pitch actuation load would need to be considered in the cost function.

Bibliography

[1] J. Lee and F. Zhao, "Global Wind Report 2021," *Global Wind Energy Council*, p. 75, 2021.

[2] "Developments of bottom-fixed offshore wind foundations in Europe." https://www.windpowerengineering.com/developments-bottom-fixed-offshore-wind-foundations-europe/. [Last accessed: 2022-2-4].

[3] C. Pearson, *Vertical Axis Wind Turbine Acoustics*. PhD thesis, Corpus Christi College Cambridge University, 2013.

[4] S. Eriksson, H. Bernhoff, and M. Leijon, "Evaluation of different turbine concepts for wind power," *Renewable and Sustainable Energy Reviews*, vol. 12, no. 5, pp. 1419–1434, 2008.

[5] D. Marten, *QBlade: A Modern Tool for the Aeroelastic Simulation of Wind Turbines vorgelegt von*. PhD thesis, TU Berlin, 2019.

[6] H. A. Madsen, U. S. Paulsen, and L. Vitae, "Analysis of vawt aerodynamics and design using the actuator cylinder flow model," in *Journal of Physics: Conference Series*, vol. 555, p. 012065, IOP Publishing, 2014.

[7] A. Van Garrel, "Development of a Wind Turbine Aerodynamics Simulation Module," *ECN Wind Energy*, no. August, p. 106, 2003.

[8] J. G. Njiri and D. Söffker, "State-of-the-art in wind turbine control: Trends and challenges," *Renewable and Sustainable Energy Reviews*, vol. 60, pp. 377–393, 2016.

[9] LeBlanc and Ferreir, "Overview and design of pitchVAWT: Vertical axis wind turbine with active variable pitch for experimental and numerical comparison," *Wind Energy Symposium, 2018*, no. 210029, pp. 1–11, 2018.

[10] A. Q. Al-Shetwi, "Sustainable development of renewable energy integrated power sector: Trends, environmental impacts, and recent challenges," *Science of The Total Environment*, p. 153645, 2022.

[11] L. Pustina, C. Lugni, G. Bernardini, J. Serafini, and M. Gennaretti, "Control of power generated by a floating offshore wind turbine perturbed by sea waves," *Renewable and Sustainable Energy Reviews*, vol. 132, no. July, p. 109984, 2020.

[12] M. Bilgili, A. Yasar, and E. Simsek, "Offshore wind power development in Europe and its comparison with onshore counterpart," *Renewable and Sustainable Energy Reviews*, vol. 15, no. 2, pp. 905–915, 2011.

[13] "Future energy industry trends." https://northsearegion.eu/northsee/e-energy/future-energy-industry-trends/. [Last accessed: 2022-2-4].

[14] W. Tjiu, T. Marnoto, S. Mat, M. H. Ruslan, and K. Sopian, "Darrieus vertical axis wind turbine for power generation i: Assessment of darrieus vawt configurations," *Renewable Energy*, vol. 75, pp. 50–67, 2015.

[15] H. Akimoto, K. Tanaka, and K. Uzawa, "Floating axis wind turbines for offshore power generationa conceptual study," *Environmental Research Letters*, vol. 6, no. 4, p. 044017, 2011.

[16] I. Paraschivoiu, *Wind turbine design: with emphasis on Darrieus concept*. Presses inter Polytechnique, 2002.

[17] Z. Cheng, H. A. Madsen, W. Chai, Z. Gao, and T. Moan, "A comparison of extreme structural responses and fatigue damage of semi-submersible type floating horizontal and vertical axis wind turbines," *Renewable Energy*, vol. 108, pp. 207–219, 2017.

[18] H. Zhu, W. Hao, C. Li, Q. Ding, and B. Wu, "A critical study on passive flow control techniques for straight-bladed vertical axis wind turbine," *Energy*, vol. 165, pp. 12–25, 2018.

[19] R. Templin and R. Rangi, "Vertical-axis wind turbine development in canada," *IEE Proceedings A (Physical Science, Measurement and Instrumentation, Management and Education, Reviews)*, vol. 130, no. 9, pp. 555–561, 1983.

[20] I. Mays, C. Morgan, M. Anderson, and S. Powles, "The 500 kw vawt 850 is now operating," *Mod. Power Syst*, vol. 10, pp. 53–55, 1990.

[21] P. South and A. Watts, "Magdalen islands vawt field test," in *Workshop on Economic and Operational Requirements and Status of Large Scale Wind Systems*, pp. 334–351, 1979.

[22] A. Choudhry, M. Arjomandi, and R. Kelso, "Methods to control dynamic stall for wind turbine applications," *Renewable Energy*, vol. 86, pp. 26–37, 2016.

[23] F. Scheurich, T. M. Fletcher, and R. E. Brown, "Simulating the aerodynamic performance and wake dynamics of a vertical-axis wind turbine," *Wind Energy*, vol. 14, no. 2, pp. 159–177, 2011.

[24] T. J. Carrigan, B. H. Dennis, Z. X. Han, and B. P. Wang, "Aerodynamic shape optimization of a vertical-axis wind turbine using differential evolution," *International Scholarly Research Notices*, vol. 2012, 2012.

[25] J. M. Bundi, X. Ban, D. W. Wekesa, and S. Ding, "Pitch control of small h-type darrieus vertical axis wind turbines using advanced gain scheduling techniques," *Renewable Energy*, vol. 161, pp. 756–765, 2020.

[26] P. Lap-Arparat and T. Leephakpreeda, "Real-time maximized power generation of vertical axis wind turbines based on characteristic curves of power coefficients via fuzzy pulse width modulation load regulation," *Energy*, vol. 182, pp. 975–987, 2019.

[27] Y. bin Liang, L. xun Zhang, E. xiao Li, and F. yue Zhang, "Blade pitch control of straight-bladed vertical axis wind turbine," *Journal of Central South University*, vol. 23, no. 5, pp. 1106–1114, 2016.

[28] F. D. Bianchi, H. De Battista, and R. J. Mantz, *Wind turbine control systems: principles, modelling and gain scheduling design*, vol. 19. Springer, 2007.

[29] G. van der Veen, J. van Wingerden, P. Fleming, A. Scholbrock, and M. Verhaegen, "Global data-driven modeling of wind turbines in the presence of turbulence," *Control Engineering Practice*, vol. 21, no. 4, pp. 441–454, 2013.

[30] S. Yin, G. Wang, and H. R. Karimi, "Data-driven design of robust fault detection system for wind turbines," *Mechatronics*, vol. 24, no. 4, pp. 298–306, 2014.

[31] W. Favoreel, B. De Moor, and M. Gevers, "Spc: Subspace predictive control," *IFAC Proceedings Volumes*, vol. 32, no. 2, pp. 4004–4009, 1999.

[32] S. T. Navalkar, J. W. Van Wingerden, E. Van Solingen, T. Oomen, E. Pasterkamp, and G. A. Van Kuik, "Subspace predictive repetitive control to mitigate periodic loads on large scale wind turbines," *Mechatronics*, vol. 24, no. 8, pp. 916–925, 2014.

[33] V. Kumar, "Repetitive control for floating offshore vertical axis wind turbine," Master's thesis, TU Delft, 2018.

[34] G. Tescione, *On the aerodynamics of a vertical axis wind turbine wake: an experimental and numerical study*. PhD thesis, TU Delft, 2016.

[35] M. Soliman, O. Malik, and D. Westwick, "Fault tolerant control of variable-speed variable-pitch wind turbines: a subspace predictive control approach," *IFAC Proceedings Volumes*, vol. 45, no. 16, pp. 1683–1688, 2012.

[36] H. Beri and Y. Yao, "Double Multiple Streamtube Model and Numerical Analysis of Vertical Axis Wind Turbine," *Energy and Power Engineering*, vol. 03, no. 03, pp. 262–270, 2011.

[37] M. Zheng, L. Guo, Y. Li, Y. Tian, H. Teng, J. Hu, Y. Zhao, and L. Yu, "Power efficiency of 5-blade drag-type vertical axis wind turbine," *Applied Solar Energy*, vol. 51, no. 3, pp. 225–231, 2015.

[38] M. M. Aslam Bhutta, N. Hayat, A. U. Farooq, Z. Ali, S. R. Jamil, and Z. Hussain, "Vertical axis wind turbine - A review of various configurations and design techniques," *Renewable and Sustainable Energy Reviews*, vol. 16, no. 4, pp. 1926–1939, 2012.

[39] R. E. Wilson and P. B. Lissaman, "Applied aerodynamics of wind power machines," *Renewable Energy*, pp. 71–120, 2018.

[40] H. Madsen, "The actuator cylinder, a flow model for vertical axis wind turbine, institute of industrial constructions and energy technology," *Aalborg University Centre*, 1982.

[41] Z. Cheng, H. A. Madsen, Z. Gao, and T. Moan, "Aerodynamic modeling of floating vertical axis wind turbines using the actuator cylinder flow method," *Energy Procedia*, vol. 94, pp. 531–543, 2016.

[42] M. Verhaegen and V. Verdult, *Filtering and system identification: a least squares approach*. Cambridge university press, 2007.

[43] I. Houtzager, J. W. Van Wingerden, and M. Verhaegen, "Fast-array recursive closed-loop subspace model identification," *IFAC Proceedings Volumes (IFAC-PapersOnline)*, vol. 15, no. PART 1, pp. 96–101, 2009.

[44] J. G. Njiri and D. Söffker, "State-of-the-art in wind turbine control: Trends and challenges," *Renewable and Sustainable Energy Reviews*, vol. 60, pp. 377–393, 2016.

[45] A. Chiuso, "The role of vector autoregressive modeling in predictor-based subspace identification," *Automatica*, vol. 43, no. 6, pp. 1034–1048, 2007.

[46] A. Chiuso and G. Picci, "Consistency analysis of some closed-loop subspace identification methods," *Automatica*, vol. 41, no. 3, pp. 377–391, 2005.

[47] H. Ali, "Sayed adaptive filters, a john wiley & sons," *Inc., publication*, 2008.

[48] G. Mercère, L. Bako, and S. Lecœuche, "Propagator-based methods for recursive subspace model identification," *Signal Processing*, vol. 88, no. 3, pp. 468–491, 2008.

[49] M. H. Hayes, "9.4: Recursive least squares," *Statistical Digital Signal Processing and Modeling*, vol. 541, p. 445, 1996.

[50] W. F. Arnold and A. J. Laub, "Generalized eigenproblem algorithms and software for algebraic riccati equations," *Proceedings of the IEEE*, vol. 72, no. 12, pp. 1746–1754, 1984.

[51] J. Frederik, L. Kröger, G. Gülker, and J.-W. van Wingerden, "Data-driven repetitive control: Wind tunnel experiments under turbulent conditions," *Control Engineering Practice*, vol. 80, pp. 105–115, 2018.

[52] F. Gustafsson and F. Gustafsson, *Adaptive filtering and change detection*, vol. 1. Citeseer, 2000.

[53] E. A. Bossanyi, *Bladed Theory Manual 4.6*, 2014.

[54] E. A. Bossanyi, "The design of closed loop controllers for wind turbines," *Wind energy: An International Journal for Progress and Applications in Wind Power Conversion Technology*, vol. 3, no. 3, pp. 149–163, 2000.

[55] B. J. Jonkman and M. L. Buhl Jr, "Turbsim user's guide," tech. rep., National Renewable Energy Lab.(NREL), Golden, CO (United States), 2006.

[56] D. A. Pollak, N. G. Nygaard, M. M. Jimémez, R. Wagner, and A. Sathe, "Characterization of ambient offshore turbulence intensity from analysis of nine offshore meteorological masts in northern europe," in *AGU Fall Meeting Abstracts*, vol. 2014, pp. GC42B–02, 2014.

Glossary

List of Acronyms

VAWT	Vertical Axis Wind Turbine
HAWT	Horizontal Axis Wind Turbine
SPC	Subspace Predictive Control
SPRC	Subspace Predictive Repetitive Control
AOA	Angle of Attack
IPC	Individual Pitch Control
MPC	Model Predictive Control
LPV	Linear Parameter Varying
TSR	Tip-Speed Ratio
MIMO	Multi Input Multi Output
LQR	Linear-Quadratic Regulator
DARE	Discrete Algebraic Riccati Equation
DMST	Double Multiple Streamtube
LLT	Lifting Line Theory
RLS	Recursive Least Square
RPBSID	Recursive Predictor-Based Subspace Identification
DARE	Discrete-time Algebraic Riccati Equation
NRMSE	Normalized Root Mean Squared Error
DLL	Dynamic-Link Library
DMST	Double Multiple Streamtube Model
AC	Actuator Cylinder
PRBS	Pseudo-Random Binary Sequence
TI	Turbulence Intensity
I/O	Inuput/Output

List of Symbols

α	Angle of attack
δ	Cut-off factor
Γ	Vortex strength
λ	Tip-speed ratio
ω	Rotational speed
θ	Azimuth angle
A	Area of the actuator disk
a	Induction factor
c	Chord length
C_{D}	Drag coefficient
C_{L}	Lift coefficient
C_{n}	Normal coefficient
C_{t}	Tangential coefficient
C_T	Thrust coefficient
F_{n}	Normal force
h	Blade height
l_0	Length of the vortex line
T	Thrust force
V_∞	Inflow wind speed
V_a	Induced velocity
V_e	Downstream velocity
V_R	Relative velocity